BULLETIN OF THE EARTHQUAKE
RESEARCH INSTITUTE
Vol. 45 (1967), pp. 1229-1294

# 54. *Electromagnetic Induction within Non-uniform Plane and Spherical Sheets.*

By Tsuneji RIKITAKE,

Earthquake Research Institute.

(Read May 23, 1967.—Received Aug. 15, 1967.)

## Summary

Computer programmes for studying electromagnetic inductions in plane and spherical sheets having any conductivity distribution are compiled. Application of the programme to a plane sheet which simulates a gradual increase in the sea-depth from the coast-line leads to a conclusion that a high concentration of the induced current takes place over the deep sea area resulting in an anomalous magnetic variation field there.

Electromagnetic induction in a spherical sheet, which represents the large-scale non-uniform conductivity distribution of the earth's surface, proves that the induced currents tend to be deflected from the low-conducting continental areas and to encircle the oceanic areas. The most remarkable current vortex takes place over the South Pacific. It seems likely that the *Sq*, *s.s.c.* and the like would be seriously affected by the induced fields, although the influence of the surface conductivity would become small to some extent if proper account is taken of the coupling between the surface sheet and the conducting mantle.

## 1. Introduction

Price[1] advanced a theory of electromagnetic induction in non-uniform thin sheets and shells. Numerous applications of the theory have subsequently followed because electromagnetic induction in thin sheets of conductor is important for a number of geophysical problems, such as shielding of the ionosphere, induction of electric currents in seas and oceans, and so on.

Electromagnetic induction by periodic and aperiodic fields in a plane sheet in which the conductivity varies periodically in a certain direction was studied by Price[1] himself. Although only a moderate

1) A. T. PRICE, *Quart. J. Mech. and Applied Math.*, **2** (1949), 283-310

conductivity contrast was considered by him, a marked tendency for induced currents to encircle the high-conducting portion of the sheet was brought out. Rikitake and Yokoyama[2] studied an induction problem in a plane sheet having a discontinuous conductivity distribution. Rikitake and Yukutake[3] and Rikitake and Sawada[4] examined electromagnetic inductions respectively in non-uniform and anisotropic plane sheets underlain by a uniform semi-infinite conductor.

Probably one of the most important applications of the Price theory for a spherical case to an actual problem would be the work by Ashour and Price[5] who studied periodic as well as aperiodic inductions in a non-uniform spherical sheet simulating the ionosphere. Rikitake and Yokoyama[2] tried to compute the electric currents induced by a uniform inducing field in a uniform hemispherical sheet by summing up spherical harmonic functions of finite number. Rikitake[6),7),8)] extended the study to induction by a hypothetical *Sq* field in an idealized hemispherical ocean. The importance of the electromagnetic coupling between a hemispherical sheet and an underlying spherical conductor was emphasized by Rikitake.[7),8),9)] Ashour[10)], who was able to obtain an exact solution for a perfectly-conducting hemispherical sheet, computed the induced currents and associated magnetic fields without neglecting any factor.

A number of different approaches to induction problems in thin sheets have also been published. Ashour[11),12)] reported on a method based on an integral equation which can be applied to electromagnetic induction in a thin conducting surface of revolution with axisymmetric conductivity by a varying magnetic field which is also symmetric about the same axis. He estimated the times of free decay in circular oceans. When the conductivity is regarded as infinitely large, there are many problems

2) T. RIKITAKE and I. YOKOYAMA, *Bull. Earthq. Res. Inst.*, **33** (1955), 297-331.
3) T. RIKITAKE, *Electromagnetism and the Earth's Interior*. Elsevier Pub. Co. Amsterdam (1966).
4) T. RIKITAKE and M. SAWADA, *Bull. Earthq. Res. Inst.*, **40** (1962), 657-683.
5) A. A. ASHOUR and A. T. PRICE, *Proc. Roy. Soc. London* ser. A, **195** (1948), 198-224.
6) T. RIKITAKE, *J. Geomag. Geoelectr.*, **11** (1960), 65-79.
7) T. RIKITAKE, *J. Geophys. Res.*, **66** (1961), 3245-3254.
8) T. RIKITAKE, *J. Geophys. Res.*, **67** (1962), 2588-2591.
9) T. RIKITAKE, *Geophys. J.*, **5** (1961), 1-15.
10) A. A. ASHOUR, *Geophys. J.*, **10** (1965), 147-161.
11) A. A. ASHOUR, *Quart. J. Mech. and Applied Math.*, **3** (1950), 119-128.
12) A. A. ASHOUR, *Quart. J. Mech. and Applied Math.*, **18** (1965), 73-86.

to which conformal mapping[13], relaxation[14] and other methods[15] can readily be applied.

Turning to the observational side of geomagnetism, a number of findings which may possibly be accounted for by electromagnetic induction effect in the sea-water or near-surface conductors have been brought forth. As has been summarized by the present writer[3], marked anomalies of geomagnetic variation that certainly reflect anomalies of the electrical conductivity in the earth's crust or upper mantle have recently been reported. Some of them, e.g. the Californian coast anomaly as reported by Schmucker[13] and the Australian anomaly by Parkinson[16),17),18], seem to be seriously affected by electric currents induced in the oceans.

Such findings stimulated theoretical investigations of the "coast effect" or "edge effect" of oceans on geomagnetic variations as already reviewed in the foregoing paragraphs. It appears to the writer, however, that the actual extent of coast or edge effect is still not quite clear even in the cases of the best examples like the Californian and Australian anomalies. It is also possible that these anomalies are strongly affected by undulations of a highly-conducting mantle. As for a much more complicated anomaly like the Central Japan anomaly[19], it is even more difficult to separate anomaly due to the ocean from that arising from the underground agency.

It may be said that, as far as the theoretical studies on edge effect of an ocean so far made are concerned, only qualitative investigations have been put forward. In order to be more quantitative, a more realistic model of ocean should be taken into consideration. In the writer's opinion, for instance, gradual increase in the depth of sea from coast-lines should be properly taken into account. In contrast to treatments assuming sharp boundaries of conductors as hitherto made by a number of authors, mathematical difficulties would increase tremendously in such a case. But recent development of high-speed computer facilitates us to tackle such problems.

It is the writer's intention in this paper to formulate the theory of electromagnetic induction within non-uniform thin sheets in such a

13) U. SCHMUCKER, *J. Geomag. Geoelectr.*, **15** (1964), 193-221.
14) T. RIKITAKE *J. Geomag. Geoelectr.*, **16** (1964), 31-36.
15) R. B. RODEN, *Geophys. J.*, **8** (1964), 375-388.
16) W. D. PARKINSON, *Geophys. J.*, **2** (1959), 1-14.
17) W. D. PARKINSON, *Geophys. J.*, **4** (1962), 441-449.
18) W. D. PARKINSON, *J. Geomag. Geoelectr.*, **15** (1964), 222-226.
19) T. RIKITAKE, *Geophys. J.*, **2** (1959), 276-287.

way as to be readily programmed for a high-speed computer. The theory more or less follows that originally advanced by Price[1].

This paper will be divided into two parts. In Part 1 will be advanced a theory of induction in a plane sheet. A computer programme only for a case in which the conductivity varies periodically in one direction will be compiled. The programme will easily be extended to cases for any distribution of conductivity. It is recognized, however, that such a generalization will require a tremendous amount of time for computation. As the main interest in Part 1 is an application of the theory to the edge effect of an ocean, it is decided to formulate a general theory which is applicable to any distribution of conductivity in Part 2 in which induction problems in a spherical sheet will be discussed in fair detail.

The theory of plane-sheet induction will be described in Section 1 of Part 1. How to modify the theory in such a way as to fit in the computer work will be indicated in Subsections 1-1 and 1-2 respectively for periodic and aperiodic inducing fields. Section 2, which consists of a number of subsections, will be reserved for actual application of the theory to a non-uniform sheet which might represent a realistic land-to-deep sea model. A fairly large conductivity contrast, 1 : 100 say, with a gradual transition from the low to high conductivity will be studied. In Section 3, the writer will discuss what is expected in geomagnetic fluctuations around the margin of an ocean on the basis of the present analysis.

In the hope of examining the effect of conductivity contrast represented by the land-sea distribution over the surface of the earth as a whole, the writer will aim at extending the theory to a non-uniform spherical sheet in Part 2 of this paper. The considerations in Part 2 will be much the same as those of Part 1. A theory that can be applicable to inductions by periodic and aperiodic inducing fields will be advanced in Section 1. In addition to these fields, an account on induction by a rotating inducing field, which may represent an idealized solar daily variation field (*Sq*-field) will be mentioned in Subsection 1-1-1. In applications of the theory which will be dealt with in Section 2, a conductivity distribution which is formed from a world's bathymetric chart will be taken into account. The conductivity contrast will reach almost 1 : 10000 at maximum. A few points, which interest the writer, will be summarized in Section 3 on the basis of the present analysis. It will be anticipated, however, that we will not be able to say anything in great detail because the time-consuming computer work prohibits

taking too many spherical harmonic functions into account.

## Part. 1. Non-uniform Plane Sheets.

### 1. Theory

Price[1] has shown that electromagnetic induction within a plane sheet by a given inducing potential $W_e$ reduces to a problem of finding an induced potential $W_i$ which satisfies

$$\nabla^2 W_i = 0 \tag{1}$$

outside the sheet and vanishes at infinity. $W_i$ must satisfy the following relation at the sheet ($z=0$) ;

$$-\rho(\partial^2 W_i/\partial z^2)_+ + \text{grad}\ \rho \cdot \text{grad}\ W_{i+} = -2\pi\partial(\partial W_e/\partial z + \partial W_i/\partial z)/\partial t, \tag{2}$$

in which subscript + denotes quantities on the plus side of the sheet and $\rho$ is the reciprocal of the electrical conductivity integrated over the thickness of the sheet.

A current function $\Psi$ of the induced electric current may be defined by

$$\Psi = (1/2\pi)\, W_{i+} . \tag{3}$$

When the resistance varies periodically in the $x$-direction and the inducing field is uniform in the same direction, a typical inducing field and the corresponding induced filed can be given as

$$W_e = A\, e^{-qz} \cos qy, \tag{4}$$

$$W_i = \cos qy \sum_{m=0}^{\infty} e^{\sqrt{m^2p^2+q^2}z}(i_{mc} \cos mpx + i_{ms} \sin mpx). \tag{5}$$

On writing the current function as

$$\Psi = \cos qy \sum_{m=0}^{\infty} (K_{mc} \cos mpx + K_{ms} \sin mpx), \tag{6}$$

(3) leads to

$$i_{mc} = 2\pi K_{mc},\ i_{ms} = 2\pi K_{ms}. \tag{7}$$

The condition as given by (2) is then written as

$$\sum_{m=0}^{\infty}[\rho(m^2p^2+q^2)\cos mpx+(d\rho/dx)mp\sin mpx]K_{mc}$$
$$+\sum_{m=0}^{\infty}[\rho(m^2p^2+q^2)\sin mpx-(d\rho/dx)mp\cos mpx]K_{ms}$$
$$=\partial\Big[Aq-2\pi\sum_{m=0}^{\infty}\sqrt{m^2p^2+q^2}(K_{mc}\cos mpx+K_{ms}\sin mpx)\Big]/\partial t, \tag{8}$$

solving which $K_{mc}$'s and $K_{ms}$'s are to be determined.

Multiplying (8) by $\cos Mpx$ and integrating it with respect to $x$ from $-\pi/p$ to $\pi/p$, we obtain

$$\sum_{m=0}^{\infty}\Big[(m^2p^2+q^2)\int_{-\pi/p}^{\pi/p}\rho(x)\cos mpx\cos Mpxdx$$
$$+mp\int_{-\pi/p}^{\pi/p}(d\rho/dx)\sin mpx\cos Mpxdx\Big]K_{mc}$$
$$+\sum_{m=0}^{\infty}\Big[(m^2p^2+q^2)\int_{-\pi/p}^{\pi/p}\rho(x)\sin mpx\cos Mpxdx$$
$$-mp\int_{-\pi/p}^{\pi/p}(d\rho/dx)\cos mpx\cos Mpxdx\Big]K_{ms}$$
$$=\begin{cases}(2\pi/p)d[Aq-2\pi qK_{0c}]/dt & \text{for } M=0\\ -(\pi/p)2\pi\sqrt{M^2p^2+q^2}dK_{Mc}/dt & \text{for } M>0,\end{cases} \tag{9}$$

When $\rho$ is measured in units of a typical resistance $\rho_0$, we put

$$\rho_1=\rho/\rho_0 \tag{10}$$

and (9) is rewritten

$$\sum_{m=0}^{\infty}\Big[\Big\{A_1(m,M)+A_3(m,M)\Big\}K_{mc}+\Big\{B_1(m,M)-B_3(m,M)\Big\}K_{ms}\Big]$$
$$=\begin{cases}(2\pi/\rho_0p)(q/p)d(A-2\pi K_{0c})/dt & \text{for } M=0\\ -(2\pi^2/\rho_0p)\sqrt{M^2+q^2/p^2}dK_{Mc}/dt & \text{for } M>0,\end{cases} \tag{11}$$

where

$$\left.\begin{aligned}A_1(m,M)&=(m^2+q^2/p^2)\int_{-\pi}^{\pi}\rho_1(s)\cos ms\cos Msds,\\ A_3(m,M)&=m\int_{-\pi}^{\pi}(d\rho_1/ds)\sin ms\cos Msds,\\ B_1(m,M)&=(m^2+q^2/p^2)\int_{-\pi}^{\pi}\rho_1(s)\sin ms\cos Msds,\\ B_3(m,M)&=m\int_{-\pi}^{\pi}(d\rho_1/ds)\cos ms\cos Msds.\end{aligned}\right\} \tag{12}$$

A similar multiplication and integration procedure by sin $Mpx$ leads to

$$\sum_{m=0}^{\infty}\left[\left\{A_2(m,M)+A_4(m,M)\right\}K_{mc}+\left\{B_2(m,M)-B_4(m,M)\right\}K_{ms}\right]$$
$$=\begin{cases}0 & \text{for } M=0\\ -(2\pi^2/\rho_0 p)\sqrt{M^2+q^2/p^2}\,dK_{Ms}/dt & \text{for } M>0,\end{cases} \tag{13}$$

where

$$\left.\begin{aligned}A_2(m,M)&=(m^2+q^2/p^2)\int_{-\pi}^{\pi}\rho_1(s)\cos ms\sin Msds,\\ A_4(m,M)&=m\int_{-\pi}^{\pi}(d\rho_1/ds)\sin ms\sin Msds,\\ B_2(m,M)&=(m^2+q^2/p^2)\int_{-\pi}^{\pi}\rho_1(s)\sin ms\sin Msds,\\ B_4(m,M)&=m\int_{-\pi}^{\pi}(d\rho_1/ds)\cos ms\sin Msds.\end{aligned}\right\} \tag{14}$$

(11) and (13) provide a set of simultaneous differential equations solving which $K_{mc}$'s and $K_{ms}$'s may be determined.

*1-1. Periodic variation*

When the inducing field is purely periodic, we put

$$d/dt=i\alpha,\quad(\alpha=2\pi/T,\ i=\sqrt{-1}) \tag{15}$$

where $T$ is the period. In such a case, let us also put

$$\left.\begin{aligned}K_{mc}&=\overline{K}_{mc}+iK^*_{mc},\\ K_{ms}&=\overline{K}_{ms}+iK^*_{ms}.\end{aligned}\right\} \tag{16}$$

Introducing (16) into (11) and (13), we obtain

$$\left.\begin{aligned}&\sum_{m=0}^{\infty}[(A_1+A_3)\overline{K}_{mc}+(B_1-B_3)\overline{K}_{ms}]-2\pi\beta\varepsilon\sqrt{M^2+q^2/p^2}K^*_{Mc}=0,\\ &\sum_{m=0}^{\infty}[(A_1+A_3)K^*_{mc}+(B_1-B_3)K^*_{ms}]+2\pi\beta\varepsilon\sqrt{M^2+q^2/p^2}\,\overline{K}_{Mc}=2\beta\gamma(q/p)A,\\ &\sum_{m=0}^{\infty}[(A_2+A_4)\overline{K}_{mc}+(B_2-B_4)\overline{K}_{ms}]-2\pi\beta\delta\sqrt{M^2+q^2/p^2}K^*_{Ms}=0,\\ &\sum_{m=0}^{\infty}[(A_2+A_4)K^*_{mc}+(B_2-B_4)K^*_{ms}]+2\pi\beta\delta\sqrt{M^2+q^2/p^2}\,\overline{K}_{Ms}=0,\end{aligned}\right\} \tag{17}$$

in which

$$\left.\begin{aligned}&\beta=\pi\alpha/\rho_0 p,\\&\gamma=1 \text{ for } M=0,\ \gamma=0 \text{ for } M>0,\\&\delta=0 \text{ for } M=0,\ \delta=1 \text{ for } M>0,\\&\varepsilon=2 \text{ for } M=0,\ \varepsilon=1 \text{ for } M>0.\end{aligned}\right\} \tag{18}$$

(17) provides a set of simultaneous equations of infinite number with unknowns also of infinite number. It is possible, however, to solve them so long as high degree terms are assumed to be ignored. Examples of solutions for $m=0, 1, 2, \ldots, 11$ will be given in a later section.

*1-2. Aperiodic variation*

A method of obtaining an approximate solution for an aperiodic inducing field may be the following one which is readily programmed for a high-speed computer.

Going back to (11), its difference form is approximately written as

$$\begin{aligned}&\sum_{m=0}^{\infty}[\{A_1(m, M)+A_3(m, M)\}K_{mc}(t)+\{B_1(m, M)-B_3(m, M)\}K_{ms}(t)]\\&=\begin{cases}\dfrac{1}{\Delta t}\dfrac{2\pi}{\rho_0 p}\dfrac{q}{p}[A(t+\Delta t)-A(t)-2\pi\{K_{0c}(t+\Delta t)-K_{0c}(t)\}] & \text{for } M=0\\ -\dfrac{1}{\Delta t}\dfrac{2\pi^2}{\rho_0 p}\sqrt{M^2+q^2/p^2}\{K_{Mc}(t+\Delta t)-K_{Mc}(t)\} & \text{for } M>0,\end{cases}\end{aligned} \tag{19}$$

from which we obtain

$$\begin{aligned}K_{0c}(t+\Delta t)=K_{0c}(t)&-\frac{p}{2Cq}\sum_{m=0}^{\infty}[\{A_1(m, 0)+A_3(m, 0)\}K_{mc}(t)\\&+\{B_1(m, 0)-B_3(m, 0)\}K_{ms}(t)]-\{A(t+\Delta t)-A(t)\}/2\pi \qquad \text{for } M=0,\end{aligned} \tag{20}$$

$$\begin{aligned}K_{Mc}(t+\Delta t)=K_{Mc}(t)&-\frac{1}{C\sqrt{M^2+q^2/p^2}}\sum_{m=0}^{\infty}[\{A_1(m, M)+A_3(m, M)\}K_{mc}(t)\\&+\{B_1(m, M)-B_3(m, M)\}K_{ms}(t)] \qquad \text{for } M>0,\end{aligned} \tag{21}$$

and similarly

$$\begin{aligned}K_{Ms}(t+\Delta t)=K_{Ms}(t)&-\frac{1}{C\sqrt{M^2+q^2/p^2}}\sum_{m=0}^{\infty}[\{A_2(m, M)+A_4(m, M)\}K_{mc}(t)\\&+\{B_2(m, M)-B_4(m, M)\}K_{ms}(t)] \qquad \text{for } M>0,\end{aligned} \tag{22}$$

where

$$C=\frac{2\pi^2}{\Delta t\rho_0 p}. \tag{23}$$

As $A_1$, $A_2$, $A_3$, $A_4$, $B_1$, $B_2$, $B_3$ and $B_4$ for various combinations of $m$ and $M$ can be computed on the basis of (12) and (14), coefficients of the current function at $t+\Delta t$ can approximately be obtained from those at $t$ provided $\Delta t$ is sufficiently small.

It is hard to generally discuss the accuracy of the above method. But a rough idea about the accuracy can be obtained from an induction within a uniform sheet. In such a case, it is obvious that $M=0$ and $K_{ms}=0$ for an inducing field of the type given by (4).

Putting $p=q$, $A=0$ (no inducing field) and $K_{0c}(0)=1$, free decay of the initially excited currents will be studied in the following. (20) reduces to

$$K_{0c}(t+\Delta t)=(1-\pi/C)K_{0c}(t), \tag{24}$$

because $A_1=2\pi$ and $A_3=B_1=B_3=0$ in this case. Meanwhile the exact solution of the free decay is given as

$$K_{0c}(t)=e^{-\frac{\rho_0 p}{2\pi}t}. \tag{25}$$

On taking $C$ in such a way as to make $\pi/C=0.01$, the approximate values of $K_{0c}$ for a number of $t$'s are calculated from (24) as given in Table 1 in which the exact values are also indicated.

Table 1. Comparison between the approximate and exact solutions.

| $t$ | Appr. sol. | Exact sol. |
|---|---|---|
| 0 | 1.0000 | 1.0000 |
| 10 $\Delta t$ | 0.9044 | 0.9048 |
| 20 $\Delta t$ | 0.8179 | 0.8187 |
| 40 $\Delta t$ | 0.6690 | 0.6703 |
| 60 $\Delta t$ | 0.5471 | 0.5488 |
| 80 $\Delta t$ | 0.4475 | 0.4493 |
| 100 $\Delta t$ | 0.3660 | 0.3679 |

It is therefore concluded that the approximate method gives fairly accurate solutions provided time-interval $\Delta t$ is so small that $\pi/C$ is less than 0.01 or so. Even in cases of non-uniform sheet, the method may work with an accuracy not largely different from that discussed in the above.

## 2. Application of the theory

### *2-1. Resistance distribution*

The resistance is assumed to vary periodically in the $x$-direction. In order to apply the theory to any resistance distribution, the computer programme is compiled so as to read the resistance values from $-px$ to $px$ with an interval $2\pi/100$. Judging from the computer time needed for the following computations, it does not seem practicable to adopt a much smaller interval.

The derivative of the resistance at the $i$-th point is then computed by

$$\left(\frac{d\rho}{dx}\right)_i=\frac{1}{\Delta x}\left[\frac{\rho_{i+1}-\rho_{i-1}}{2}-\frac{1}{6}\,\frac{\rho_{i+2}-2\rho_{i+1}+2\rho_{i-1}-\rho_{i-2}}{2}\right], \tag{26}$$

where $\rho_i$ is the resistance at the $i$-th point and $\Delta x$ is the interval. In the actual work, $\rho$ is replaced by the normalized resistance $\rho_1$ as defined by (10).

As it is intended to apply the present study to examining the edge effect of an ocean, a fairly large contrast between the high and low conducting portions is assumed. Taking into consideration the fact that a sea gets gradually deeper from the coast-line, it is also assumed that the transition from the low to high conducting portion is linear. In the actual calculation the following is taken:

$$\left.\begin{aligned}
&\rho_1=1 && \text{for } -\pi<px<-\pi/2,\\
&\rho_1=1-\frac{4.95}{\pi}(px+\pi/2) && \text{for } -\pi/2<px<-3\pi/10,\\
&\rho_1=0.01 && \text{for } -3\pi/10<px<3\pi/10,\\
&\rho_1=0.01+\frac{4.95}{\pi}(px-3\pi/10) && \text{for } 3\pi/10<px<\pi/2,\\
&\rho_1=1 && \text{for } \pi/2<px<\pi.
\end{aligned}\right\} \tag{27}$$

The change in $\rho_1$ for $-\pi<px<\pi$ along the $x$-axis is illustrated in Fig. 1.

### *2-2. Computation of the integrals in (12) and (14)*

With $\rho_1$ and $d\rho_1/dx$ determined in the last subsection, the integrals involved in (12) and (14) are computed. As the ordinary Simpson method of integration leads to an inaccurate result when the integrand is highly

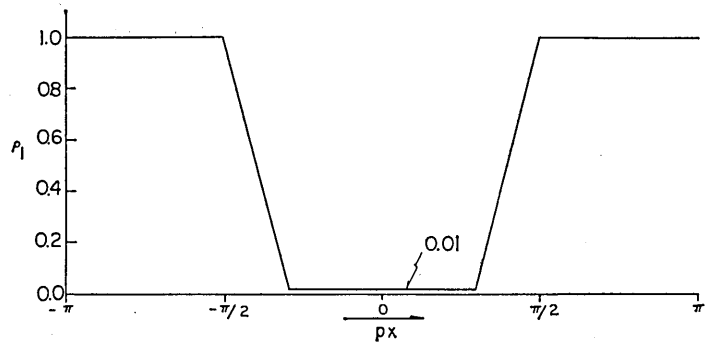


Fig. 1. The variation of the dimensionless resistance $\rho_1$ along the $x$-axis.

oscillatory, most of the numerical integrations are performed by making use of the Filon method[20] although the Simpson method is also made use of when needed. Computations are made only for $m=0\sim11$ and $M=0\sim11$ because of time-consuming computer work.

*2-3. Simultaneous equations*

In the case of induction by a periodic field, the above procedure leads to a set of simultaneous equations, 48 in number, which are solved by making use of a subprogramme compiled by Hagiwara[21]. The method is essentially a "sweep-out" one.

*2-4. Examples of induction by periodic inducing fields*

$p=q$ is assumed throughout the present paper. Assuming that the electrical conductivity of the land amounts to $10^{-13}$ e.m.u., the total conductivity integrated over a 10 km thickness becomes $10^{-7}$ e.m.u. In that case $\rho$ is estimated as $10^{7}$ e.m.u. We may hence take $\rho_0=10^{7}$ e.m.u.

If we further assume an inducing field having a wavelength of 40 degrees in longitude at middle latitude, 38° in latitude say, half wavelength $1/p$ is estimated as $0.5577\times10^{8}$ cm. These numerals lead to

$$\rho_0 p=0.1793 \text{ e.m.u.} \tag{28}$$

What follows will hold for any combinations of $\rho_0$ and $p$ which satisfy (28).

With the parameters mentioned above, simultaneous equations (17) are solved for inducing fields having periods 1 min., 1 hour and 1 day

20) L. N. G. FILON, *Proc. Roy. Soc. Edin.*, **49** (1928-29), 38-47.
21) Y. HAGIWARA, *Bull. Earthq. Res. Inst.*, **44** (1966), 519-530.

Table 2. $K_{mc}$ and $K^*_{mc}$ for various periods.

| $m$ | $T$=1 min. | | $T$=1 hour | | $T$=1 day | |
|---|---|---|---|---|---|---|
| | $K_{mc}$ | $K^*_{mc}$ | $K_{mc}$ | $K^*_{mc}$ | $K_{mc}$ | $K^*_{mc}$ |
| 0 | 0.15240 | 0.02409 | 0.02225 | −0.00944 | 0.000074 | −0.001200 |
| 1 | −0.00575 | 0.01587 | −0.02163 | 0.02220 | −0.000074 | 0.001788 |
| 2 | 0.00008 | −0.00342 | 0.01248 | −0.01732 | 0.000044 | −0.001290 |
| 3 | 0.00131 | −0.00058 | −0.00495 | 0.01052 | −0.000018 | 0.000759 |
| 4 | −0.00039 | 0.00107 | −0.00037 | −0.00412 | −0.000001 | −0.000297 |
| 5 | −0.00040 | −0.00047 | 0.00277 | −0.00030 | 0.000010 | −0.000006 |
| 6 | 0.00038 | −0.00014 | −0.00265 | 0.00225 | −0.000020 | 0.000130 |
| 7 | −0.00003 | 0.00032 | 0.00124 | −0.00224 | 0.000005 | −0.000125 |
| 8 | −0.00017 | −0.00014 | 0.00020 | 0.00129 | −0.000001 | 0.000064 |
| 9 | 0.00013 | −0.00006 | −0.00092 | −0.00035 | −0.000002 | −0.000008 |
| 10 | −0.00002 | 0.00012 | 0.00088 | −0.00014 | 0.000002 | −0.000017 |
| 11 | −0.00003 | −0.00008 | −0.00046 | 0.00019 | −0.000001 | 0.000015 |

and unit amplitude. The solutions are given in Table 2. It is obvious from symmetry consideration that $\bar{K}_{ms}$'s and $K^*_{ms}$'s are always vanishing. The results of computation in fact give vanishingly small values for these coefficients.

The computer programme has been checked by applying it to inductions in a uniform sheet and Price's model getting satisfactory agreements. Judging from the convergencies of the coefficients of current function as given in Table 2, it can be said that these coefficients provide approximate solutions of induction within the non-uniform plane sheet considered.

*2-4-1. Distribution of the induced currents*

The distributions of induced current in the sheet are readily computed from the coefficients which are given in Table 2. In a similar fashion to Price's work[1], the stream lines of electric current at three epochs, $\alpha t=0$, $\pi/3$ and $2\pi/3$ say, are obtained. They are shown in Figs. 2, 3 and 4 respectively for $T$=1 min., 1 hour and 1 day together with the distribution section of the non-dimensional conductivity.

General features of these current distributions are much the same as what has been shown by Price[1] as they should be, although more enhanced encirclings of the currents around the high-conducting portion can be observed in the present results. This seems to be caused by the conductivity contrast which is more than one order of magnitude

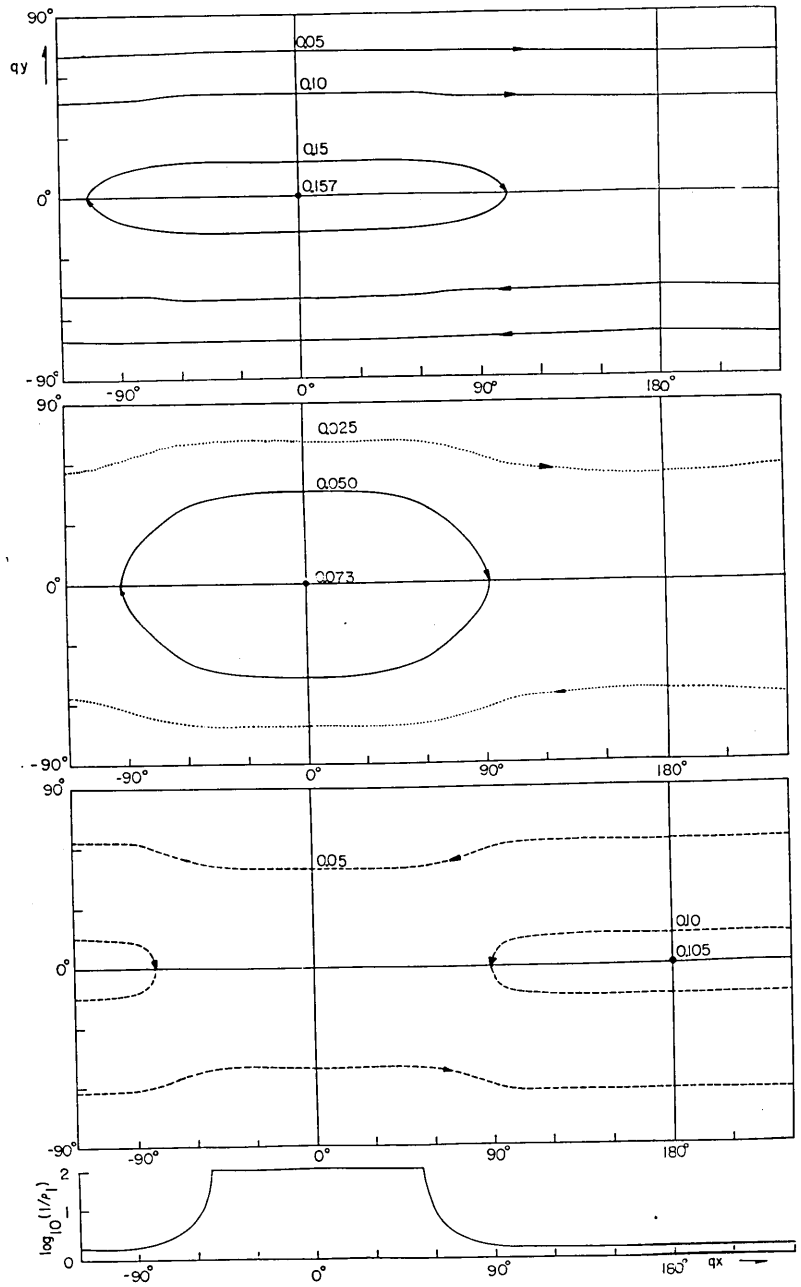


Fig. 2. Induced currents for $T=1$ min. The distribution of the dimensionless conductivity is shown at the bottom.

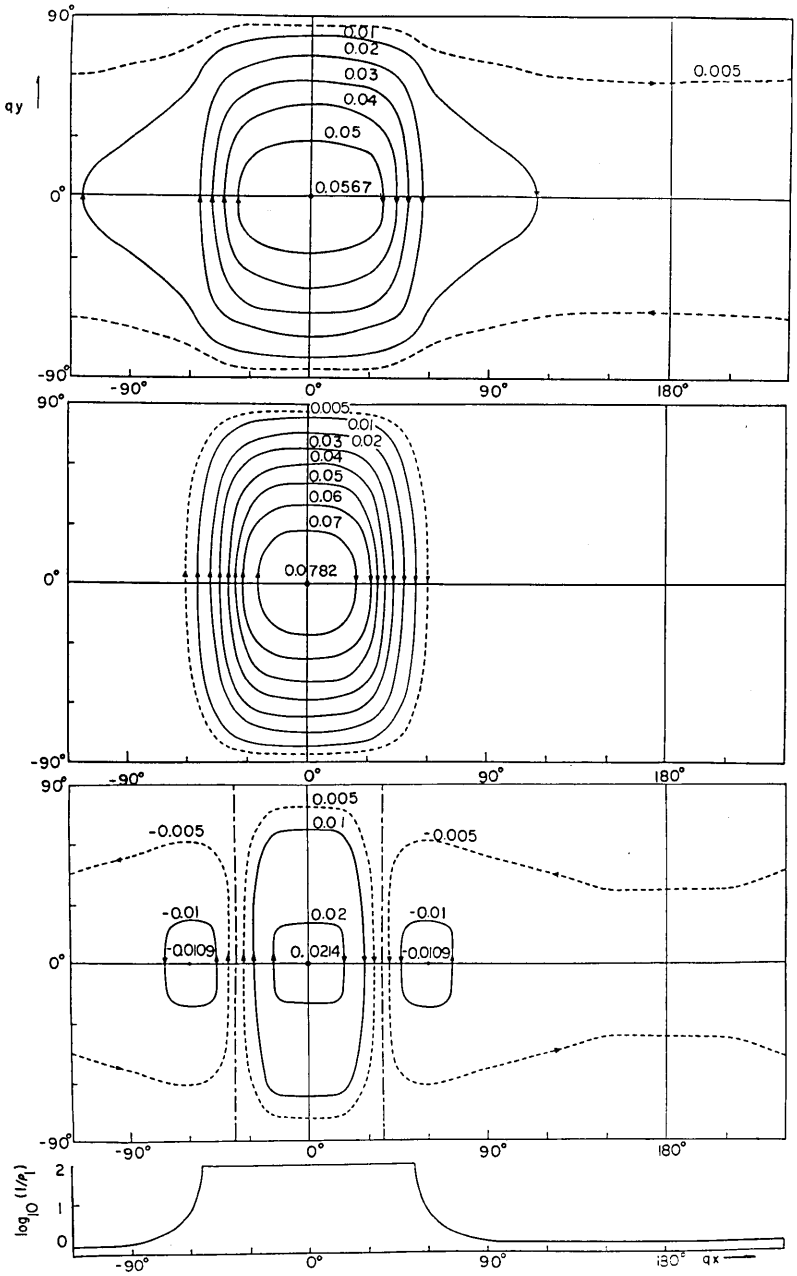


Fig. 3. Induced currents for $T=1\frac{1}{4}$ hour.

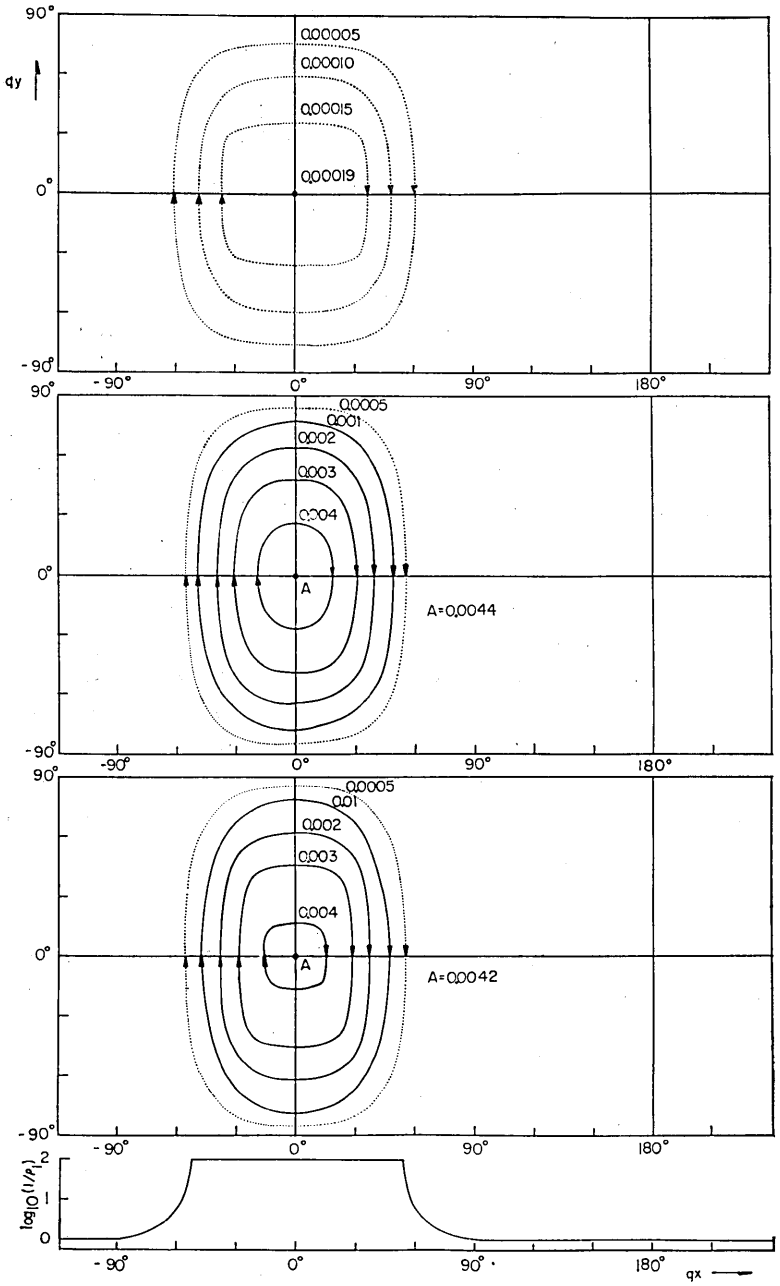


Fig. 4. Induced currents for $T=1$ day.

larger than that which was discussed by Price[1].

In the case of a rapid variation, the current intensity becomes large, but the influence of the conductivity contrast seems small, that is, the tendency for stream lines to run parallel to the $x$-axis is clearly seen in Fig. 2 which is the case for $T=1$ min. If the variation is extremely rapid or the conductivity is infinitely large, (2) becomes

$$\partial W_e/\partial z+\partial W_i/\partial z=0 \qquad \text{on } z=0\,, \tag{29}$$

so that the stream lines become exactly parallel to the $x$-axis in the present problem. It is therefore concluded that, for a rapid change in the magnetic field, the self-induction is important, so that the sheet tends to behave like a perfect conductor.

When the period is as long as 1 hour, the concentration of induced current around the high-conducting portion becomes remarkable as can be seen in Fig. 3. It is interesting to note that the concentration of current takes place over the flat part of the high-conducting portion. In other words, the current density induced in the hypothetical land-sea model is very high over the deep sea area, but a relatively small density is observed on the slope connecting the land with the deep-sea bottom.

In the event of a much longer period, $T=24$ hours say, what is stated in the above regarding the encircling and concentration may also be true although the current intensity becomes very small and the phase difference between the inducing and induced fields increases. The induced currents seem to be confined around the high-conducting portion of the sheet most of the time.

*2-4-2. Induced magnetic field*

The coefficients in Table 2 enable us to compute the components of the induced magnetic field. Figs. 5 and 6 and Figs. 7 and 8 are the demonstrations of the distribution of $X$ (parallel to the $x$-direction) and $Z$ (perpendicular to the sheet) components respectively for $T=1$ min. and 1 hour at epochs $\alpha t=0$, $\pi/3$ and $2\pi/3$.

These illustrations are of course harmonized with the current patterns in Figs. 2 and 3. It would be important to note that deviations from the field induced by the same inducing field within a uniform sheet arise around the edge of the deep-sea bottom and that very little anomaly can be observed near the boundary of land. Anomalous $Z$ component sometimes exceeds the amplitude of the inducing field.

The $Y$ components, parallel to the $y$-direction, of the inducing field

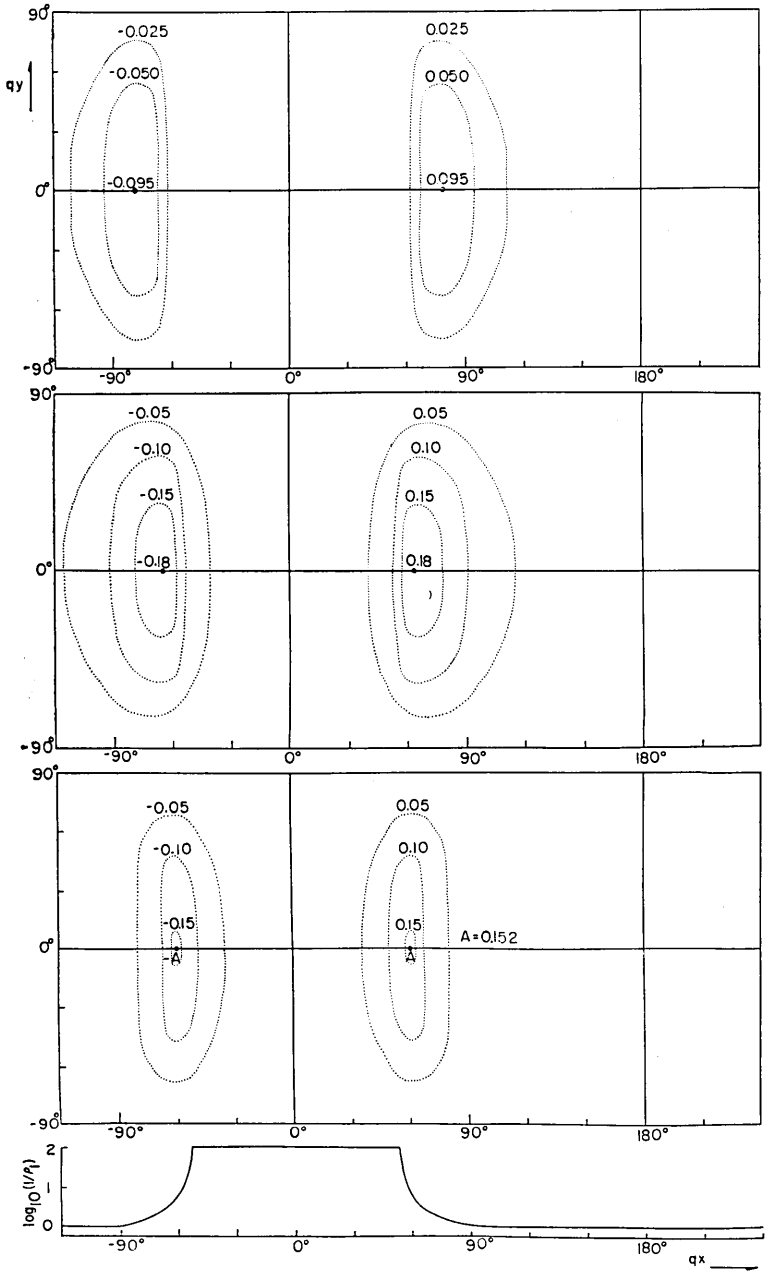


Fig. 5. Induced $X$ in units of the maximum amplitude of the inducing field for $T=1$ min.

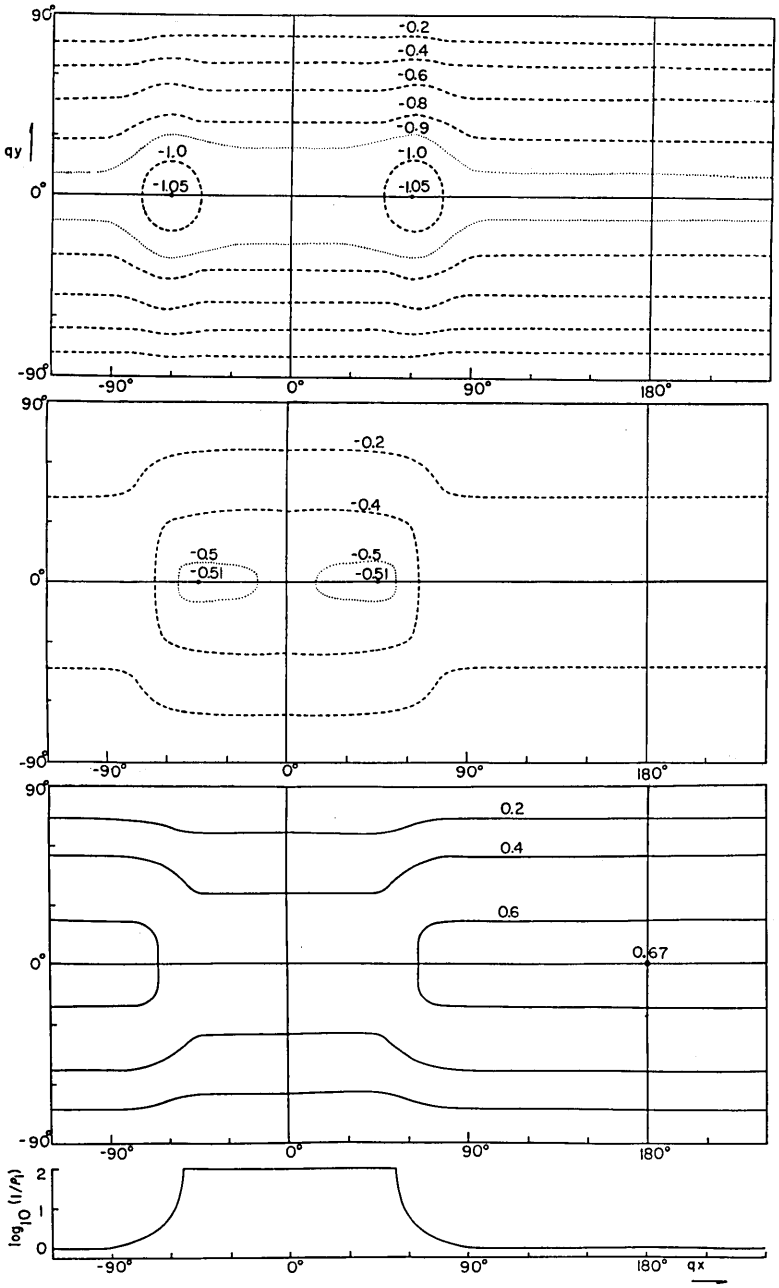


Fig. 6. Induced $Z$ for $T=1$ min.

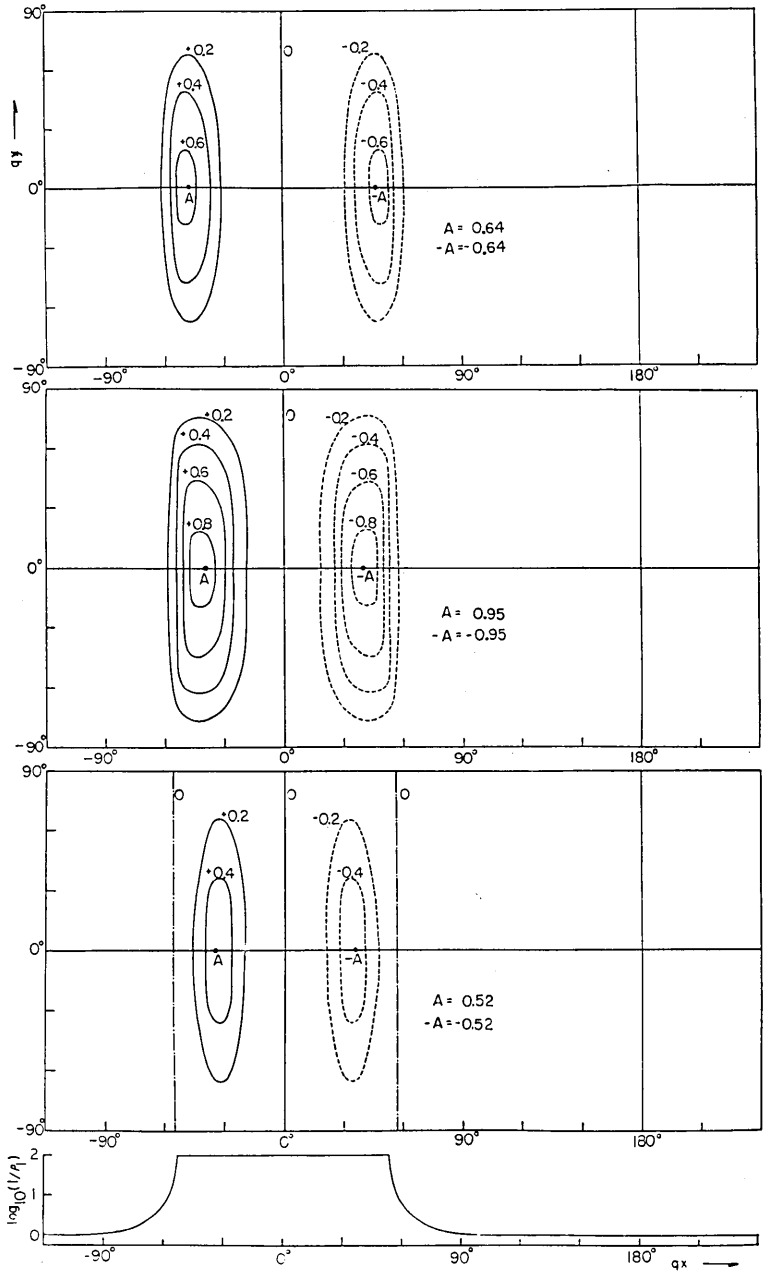


Fig. 7. Induced $X$ for $T=1$ hour.

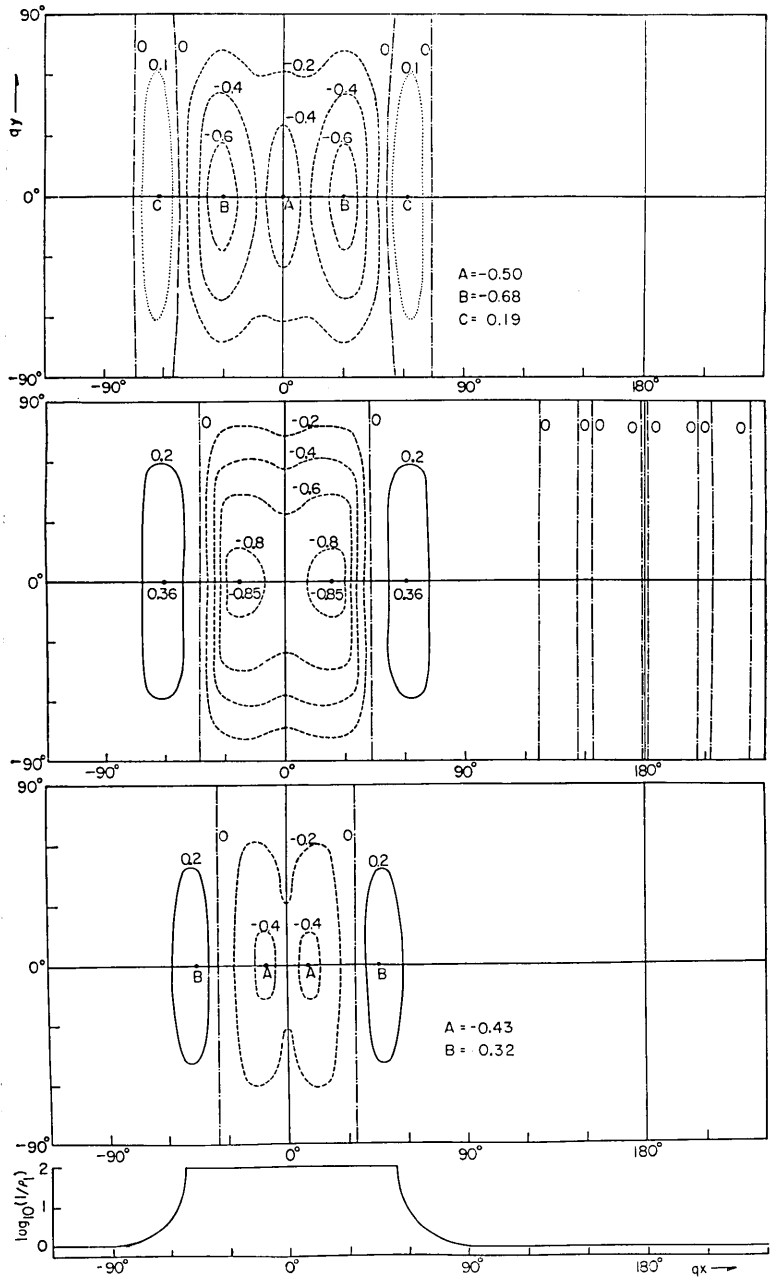


Fig. 8. Induced $Z$ for $T$=1 hour.

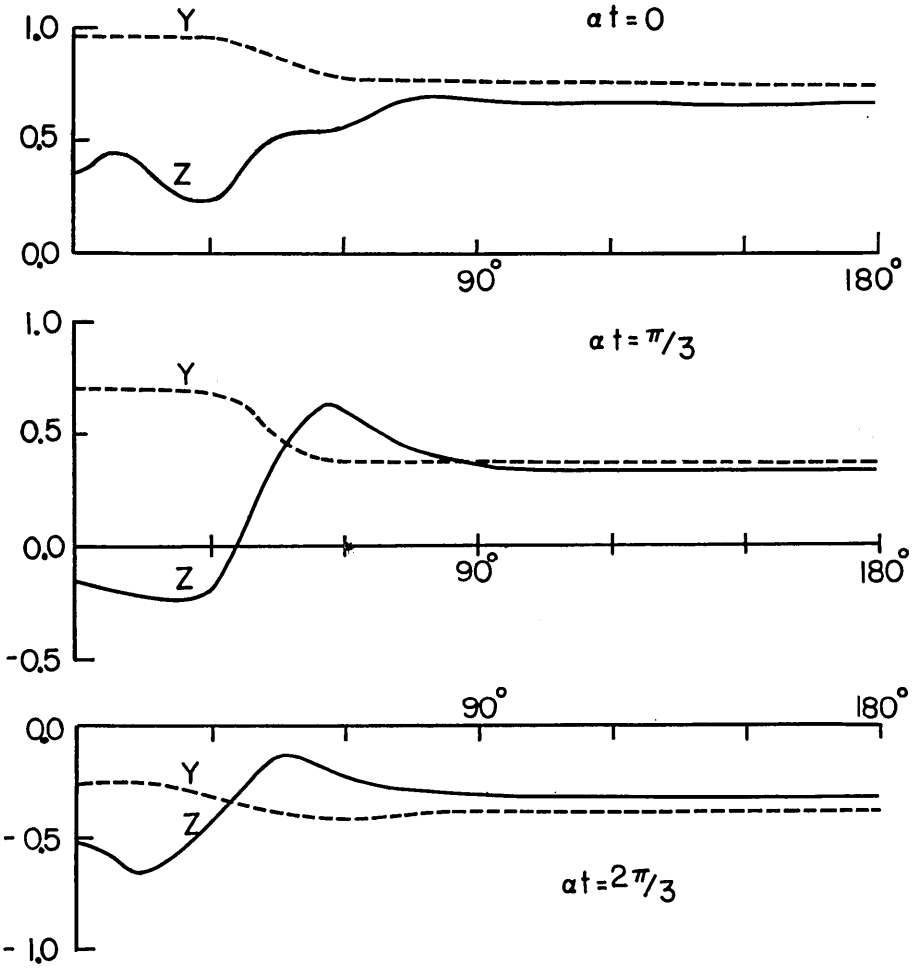


Fig. 9. The distributions of the total $Y$ and $Z$ fields on $qy=\pi/4$.

are always proportional to $\sin qy$, so that the distribution contours are parallel to the $x$-axis. In order to bring out possible edge effect of an ocean, $Y$ and $Z$ components are calculated by combining induced and inducing fields on a straight line parallel to the $x$-axis as defined by $qy=\pi/4$ for $T=1$ hour at three epochs $\alpha t=0$, $\pi/3$ and $2\pi/3$. Marked changes in the field components like reversals of sign are always seen around the edge of the flat portion of high conductivity as shown in Fig. 9. Such a fact may have an important bearing on what we call "coast effect" or "edge effect" of an ocean. Even in cases of variations of

Table 3. Time-variation of the coefficients of current function after $t=0$.

| $t$(sec.) | $K_{0c}$ | $K_{1c}$ | $K_{2c}$ | $K_{3c}$ | $K_{4c}$ | $K_{5c}$ | $K_{6c}$ | $K_{7c}$ | $K_{8c}$ | $K_{9c}$ | $K_{10c}$ | $K_{11c}$ |
|---|---|---|---|---|---|---|---|---|---|---|---|---|
| 0 | 0.1592 | 0.0000 | 0.0000 | 0.0000 | 0.0000 | 0.0000 | 0.0000 | 0.0000 | 0.0000 | 0.0000 | 0.0000 | 0.0000 |
| 10 | 0.1344 | −0.0160 | 0.0035 | 0.0008 | −0.0010 | 0.0003 | 0.0002 | −0.0002 | 0.0001 | 0.0000 | 0.0000 | 0.0000 |
| 20 | 0.1148 | −0.0268 | 0.0067 | 0.0004 | −0.0017 | 0.0010 | 0.0000 | −0.0004 | 0.0003 | −0.0001 | −0.0001 | 0.0001 |
| 30 | 0.0991 | −0.0340 | 0.0098 | −0.0005 | −0.0021 | 0.0016 | −0.0003 | −0.0004 | 0.0005 | −0.0002 | 0.0000 | 0.0001 |
| 40 | 0.0863 | −0.0387 | 0.0125 | −0.0016 | −0.0023 | 0.0027 | −0.0008 | −0.0004 | 0.0007 | −0.0005 | 0.0001 | 0.0001 |
| 50 | 0.0760 | −0.0418 | 0.0149 | −0.0028 | −0.0023 | 0.0028 | −0.0012 | −0.0003 | 0.0009 | −0.0007 | 0.0003 | 0.0000 |
| 60 | 0.0676 | −0.0437 | 0.0170 | −0.0040 | −0.0022 | 0.0033 | −0.0017 | −0.0001 | 0.0010 | −0.0009 | 0.0005 | −0.0001 |
| 70 | 0.0612 | −0.0447 | 0.0186 | −0.0050 | −0.0020 | 0.0036 | −0.0021 | 0.0001 | 0.0011 | −0.0011 | 0.0007 | −0.0002 |
| 80 | 0.0548 | −0.0453 | 0.0203 | −0.0061 | −0.0017 | 0.0039 | −0.0026 | 0.0003 | 0.0011 | −0.0013 | 0.0009 | −0.0003 |
| 90 | 0.0499 | −0.0455 | 0.0216 | −0.0071 | −0.0014 | 0.0041 | −0.0029 | 0.0006 | 0.0011 | −0.0015 | 0.0011 | −0.0004 |
| 100 | 0.0459 | −0.0454 | 0.0226 | −0.0079 | −0.0012 | 0.0043 | −0.0033 | 0.0008 | 0.0011 | −0.0017 | 0.0012 | −0.0005 |
| 110 | 0.0424 | −0.0451 | 0.0235 | −0.0086 | −0.0009 | 0.0044 | −0.0035 | 0.0009 | 0.0011 | −0.0018 | 0.0014 | −0.0006 |
| 120 | 0.0395 | −0.0448 | 0.0242 | −0.0093 | −0.0006 | 0.0045 | −0.0038 | 0.0012 | 0.0010 | −0.0019 | 0.0015 | −0.0007 |
| 130 | 0.0370 | −0.0443 | 0.0248 | −0.0099 | −0.0003 | 0.0045 | −0.0040 | 0.0014 | 0.0010 | −0.0019 | 0.0016 | −0.0007 |
| 140 | 0.0349 | −0.0438 | 0.0252 | −0.0104 | 0.0000 | 0.0045 | −0.0042 | 0.0015 | 0.0009 | −0.0020 | 0.0017 | −0.0008 |
| 150 | 0.0331 | −0.0433 | 0.0256 | −0.0108 | 0.0002 | 0.0045 | −0.0043 | 0.0017 | 0.0008 | −0.0020 | 0.0017 | −0.0008 |
| 160 | 0.0315 | −0.0428 | 0.0258 | −0.0112 | 0.0005 | 0.0045 | −0.0044 | 0.0018 | 0.0008 | −0.0020 | 0.0018 | −0.0009 |
| 170 | 0.0301 | −0.0423 | 0.0260 | −0.0115 | 0.0007 | 0.0044 | −0.0045 | 0.0020 | 0.0007 | −0.0020 | 0.0018 | −0.0009 |
| 180 | 0.0289 | −0.0418 | 0.0262 | −0.0118 | 0.0009 | 0.0043 | −0.0046 | 0.0021 | 0.0006 | −0.0019 | 0.0018 | −0.0009 |

different period, both rapid or slow, the anomalous fields arise about the same portion of the sheet.

*2-5. Free decay of induced currents*

As an example of aperiodic induction, free decay of electric currents initially induced in the sheet by a sudden change in the inducing field will be studied in this section.

At the instant ($t=0$) of a step-function type change of unit amplitude in the external field of which the magnetic potential is given in a form indicated by (4), it is obvious that $K_{0c}=1/2\pi$ and other $K_{mc}$'s and $K_{ms}$'s are all zero, so that the induced currrents flow in a direction parallel to the $x$-axis.

Taking the same conductivity distribution as that discussed in Subsection 2-4 and assuming $p=q$ as before, successive computations of (20) and (21) are performed with a time-interval $\Delta T=1$ sec. It is evident that $K_{ms}$'s are always zero. In Table 3 are given $K_{mc}$'s up to $m=11$ with an interval of 10 sec.

Changes in the coefficients of harmonics for $m=0$, 1, 2, 3, 4 and 5 are also shown in Fig. 10 in which we clearly see that $K_{0c}$ decreases monotonically, while other coefficients gradually increase and some of them tend to decrease again.

It is interesting to see how the stream lines change as time goes

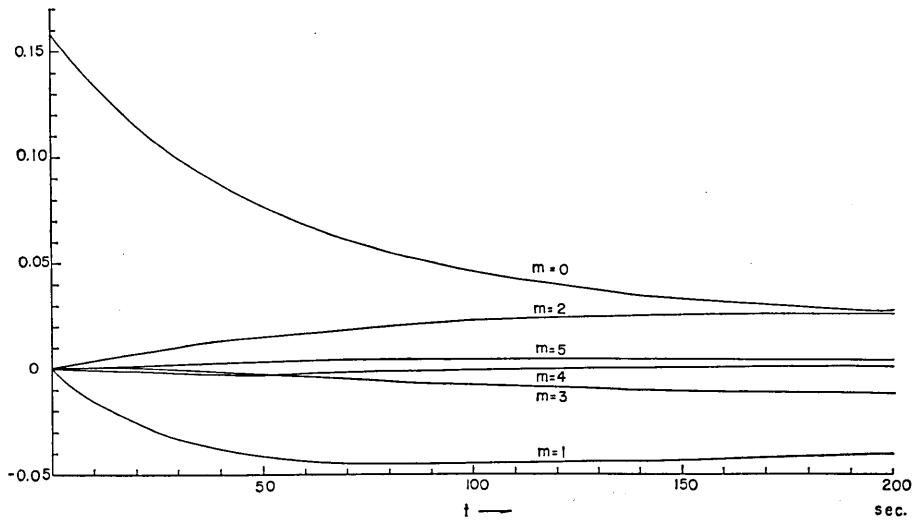


Fig. 10. Decay and development of the main current function coefficients.

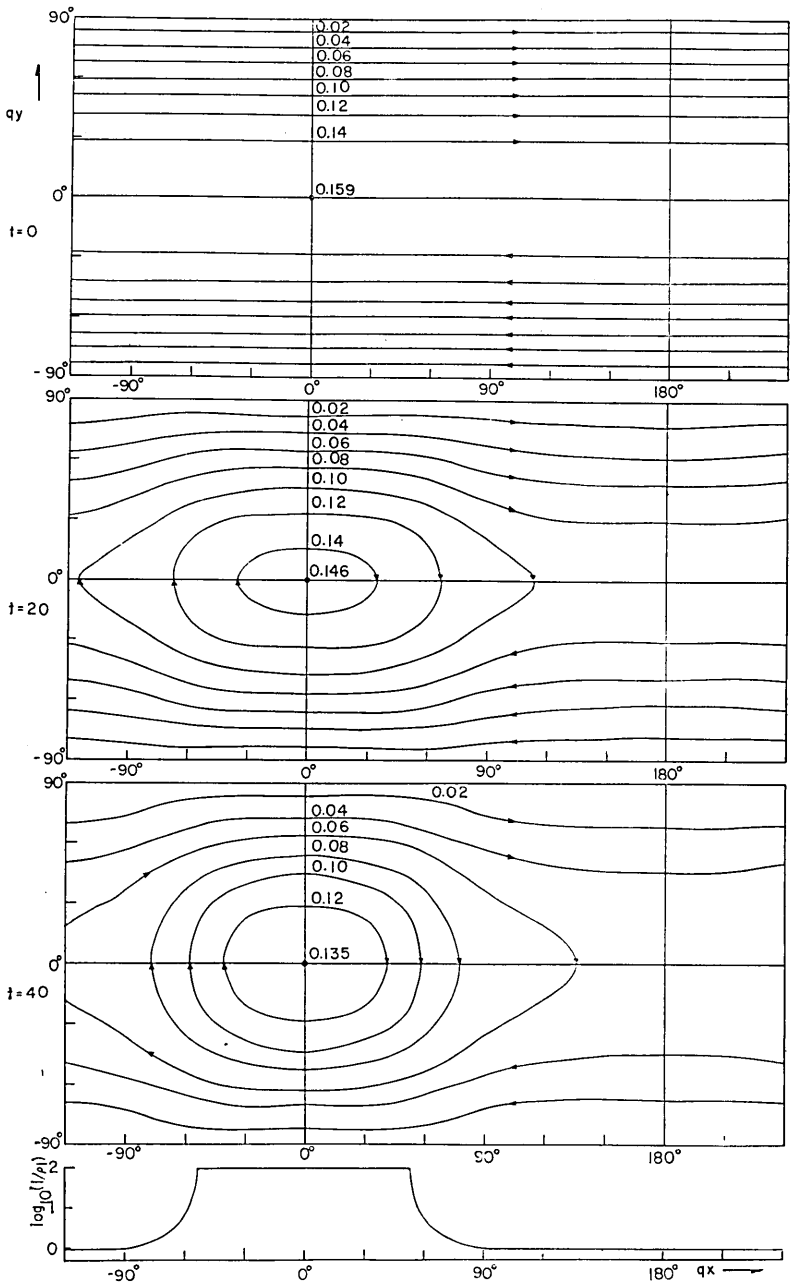


Fig. 11 a. Free decay of the induced currents.

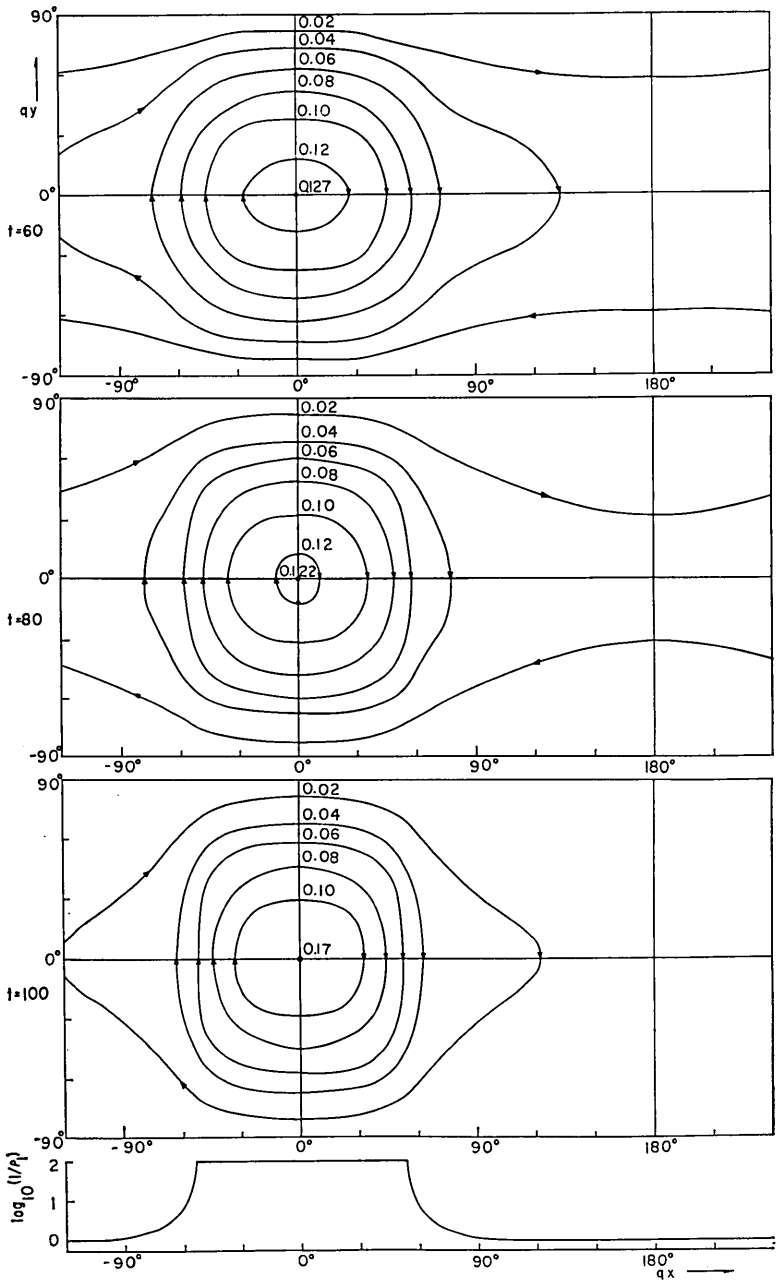


Fig. 11 b. Free decay of the induced currents.

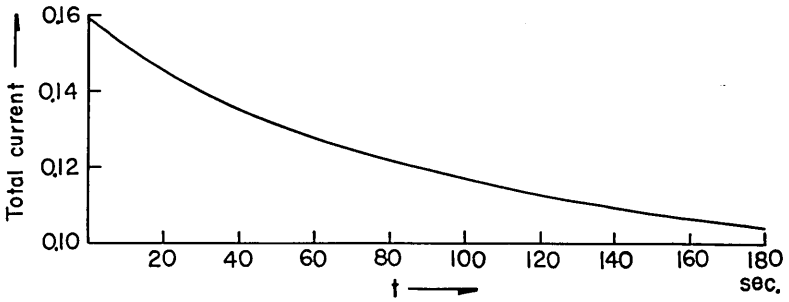


Fig. 12. Decrease in the total current.

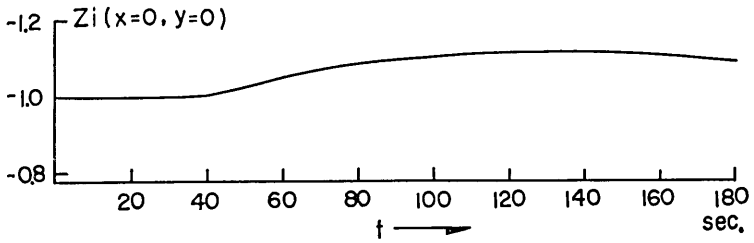


Fig. 13. Changes in the induced vertical field at $x=0$, $y=0$.

on. In Figs. 11 a and 11 b are shown the stream lines of induced current at $t=0$, 20, 40, 60, 80 and 100 sec. respectively. At $t=0$, the currents flow in a direction parallel to the $x$-axis. The density of currents tends to decrease and the currents tend to encircle the high-conducting portion of the sheet.

The total current circulating in the sheet at any time is determined by the maximum value of the current function at that time. The change in the total current is shown in Fig. 12. The rate of decay of free current-systems seems to be largely controlled by the mean conductivity as has been pointed out by Price[1].

In Fig. 13 is shown the time-variation of the $Z$ component of the induced field, which is denoted by $Z_i$, at the centre of the current vortex. At $t=0$, it is apparent that $Z_e+Z_i=0$ ($Z_e$ denotes the component vertical to the sheet of the inducing field, and so $Z_e$ is a constant in the present problem). It is seen that the relation practically holds good for some time, up to $t=30$ sec. say, because marked decrease in $Z_i$ can only be observed after $t=30$ sec. Fig. 14 indicates the changes in the total (inducing plus induced) $Y$ and $Z$ components at $qy=\pi/4$ on the

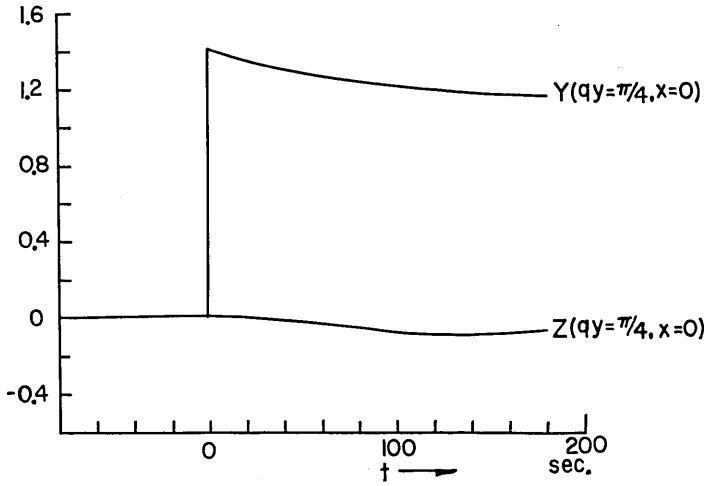


Fig. 14. Changes in the total $Y$ and $Z$ fields at $x=0$, $qy=\pi/4$.

$y$-axis. It is seen that the apparent on-set of $Z$ is delayed very much from that of $Y$. In the present case, the effect of the circulating current is so strong that reversal of $Z$ takes place. It has sometimes been noticed[22] that the on-set of $Z$ lags a few tens of seconds behind that of $H$ at particular observatories at times of *s.s.c.*'s. The above behaviour of $Z$ might provide an explanation of such an observed fact.

### 3. Discussion about the induction in the non-uniform plane sheet

One of the most important features of the induction in the present model is the strong tendency for the induced currents to encircle the high-conducting portion of the sheet. The concentration of the current is not so high over the portion which connects the high-conducting portion to the low-conducting portion. Accordingly, the anomalous magnetic fields produced by the currents occur on the high-conducting portion of the sheet. It is therefore suggested that an edge effect of an ocean on geomagnetic variations seems likely to be strong far off the coast-line and not enhanced on the land provided the gradual increase in the sea-depth is taken into account.

Fig. 15 shows the topography across north-eastern Japan along the 38° parallel circle. In so far as the Japan Islands-Pacific Ocean conductivity profile is concerned, the model studied in the above seems to

22) T. KUBOKI and H. OSHIMA, *Mem. Kakioka Mag. Obs.*, **12** (1966), 127-198, (in Japanese).

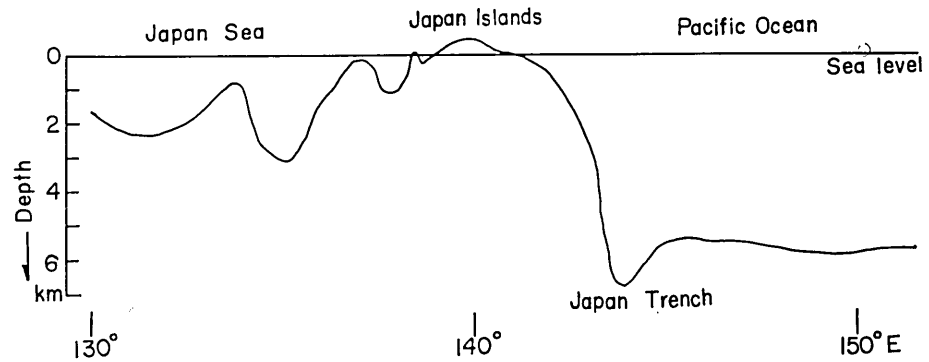


Fig. 15. East-west profile of Japan along the 38° parallel.

roughly represent the actual profile although a periodicity of the conductivity distribution has been assumed in the theory. If it is assumed that the results in the foregoing sections can be applied to the Japan Islands-Pacific Ocean profile, the high concentration of the induced electric currents would occur somewhere around the Japan Trench, probably a little outside, and so anomalous magnetic fields, especially in the $Z$ components, would be expected there. But the coast-line seems far enough from there, so that no marked anomaly would be observed on the Japan Islands.

Turning to the observed results at the magnetic observatories along the coast-line of north-eastern Japan, it has been noticed that $Z$ changes in phase with $H$ (horizontal component) but not with $D$ (declination). Should the changes be largely controlled by the electric currents induced in the ocean, it would be natural to imagine that $Z$-changes are in phase with $D$-changes because the bathymetric contours are running from north to south off north-eastern Japan. Although questions have often been raised about the possibility of accounting for the geomagnetic variation anomaly in Japan by the influence of electric currents in the seas surrounding Japan, the writer thinks that the main part of the Japanese anomaly is caused by something else, probably some agency in the upper mantle.

## Part. 2. Non-uniform Spherical Sheets.

### 1. Theory

We are going to discuss electromagnetic induction in a non-uniform

thin spherical sheet, in which the resistance is given by $\rho(\theta, \phi)$. Taking a spherical coordinate system, the sheet is denoted by $r=a$.

The magnetic potential of an inducing field is assumed as

$$W_e=ae_k^l\left(\frac{r}{a}\right)^k P_k^l(\cos\theta)\cos(l\phi+\epsilon_k^l) \qquad (r>a), \tag{30}$$

where $P_k^l(\cos\theta)$ is an associated Legendre function having degree $k$ and order $l$ as defined by Neumann.

The induced potential may be of the following form;

$$W_i=a\sum_n\sum_m(a/r)^{n+1}P_n^m(\cos\theta)(i_n^{mC}\cos m\phi+i_n^{mS}\sin m\phi) \qquad (r>a). \tag{31}$$

If the current function of electric currents induced in the sheet is denoted by

$$\Psi=\sum_n\sum_m P_n^m(\cos\theta)(K_n^{mC}\cos m\phi+K_n^{mS}\sin m\phi), \tag{32}$$

the coefficients of the induced potential are correlated to those of the current function by

$$ai_n^{mC}=4\pi\frac{n}{2n+1}K_n^{mC}, \qquad ai_n^{mS}=4\pi\frac{n}{2n+1}K_n^{mS}. \tag{33}$$

According to the theory of electromagnetic induction in a non-uniform sheet[1], the following relation should hold on the sheet:

$$\left[\frac{\partial\rho}{\partial\theta}\frac{\partial}{\partial\theta}+\frac{1}{\sin^2\theta}\frac{\partial\rho}{\partial\phi}\frac{\partial}{\partial\phi}+\frac{\rho}{\sin\theta}\frac{\partial}{\partial\theta}\left(\sin\theta\frac{\partial}{\partial\theta}\right)+\frac{\rho}{\sin^2\theta}\frac{\partial^2}{\partial\phi^2}\right]\Psi$$
$$=-a^2\frac{\partial^2}{\partial t\partial r}(W_e+W_i) \qquad \text{at } (r=a). \tag{34}$$

Putting (30) and (31) into (34) and taking (33) into account, we obtain

$$\sum_n\sum_m\frac{\partial\rho_1}{\partial\theta}\frac{dP_n^m}{d\theta}(K_n^{mC}\cos m\phi+K_n^{mS}\sin m\phi)$$
$$+\sum_n\sum_m\frac{m}{\sin^2\theta}\frac{\partial\rho_1}{\partial\phi}P_n^m(-K_n^{mC}\sin m\phi+K_n^{mS}\cos m\phi)$$
$$-\sum_n\sum_m n(n+1)\rho_1P_n^m(K_n^{mC}\cos m\phi+K_n^{mS}\sin m\phi)$$
$$=-\beta\left[ake_k^lP_k^l\cos(l\phi+\epsilon_k^l)-4\pi\sum_n\sum_m\frac{n(n+1)}{2n+1}P_n^m(K_n^{mC}\cos m\phi+K_n^{mS}\sin m\phi)\right], \tag{35}$$

where, putting time operator as $\partial/\partial t=p$, we write

$$\beta=ap/\rho_0, \qquad \rho_1=\rho/\rho_0. \tag{36}$$

$\rho_0$ is a constant having a dimension of resistance in the sheet, while $\beta$ and $\rho_1$ are dimensionless.

If we multiply both the sides of (35) by $P_N^M \sin\theta\cos M\phi$ and integrate it with respect to $\theta$ and $\phi$ respectively from $\theta=0$ to $\theta=\pi$ and from $\phi=0$ to $\phi=2\pi$, we obtain

$$\sum_n\sum_m [(A_N^{MC}-C_N^{MC}-E_N^{MC})K_n^{mC}+(B_N^{MC}+D_N^{MC}-F_N^{MC})K_n^{mS}]$$
$$=\begin{cases} -\beta\left[aNe_N^M\cos\epsilon_N^M\dfrac{2\pi}{2N+1}\dfrac{(N+M)!}{(N-M)!}-8\pi^2\dfrac{N(N+1)}{(2N+1)^2}\dfrac{(N+M)!}{(N-M)!}K_N^{MC}\right] \\ \qquad \text{for } k=N, \quad l=M \\ 8\beta\pi^2\dfrac{N(N+1)}{(2N+1)^2}\dfrac{(N+M)!}{(N-M)!}K_N^{MC} \\ \qquad \text{for other combinations of } N \text{ and } M, \end{cases} \tag{37}$$

where

$$\left.\begin{aligned} A_N^{MC}&=\int_0^\pi\int_0^{2\pi}\frac{\partial\rho_1}{\partial\theta}\frac{dP_n^m}{d\theta}P_N^M\sin\theta\cos m\phi\cos M\phi d\theta d\phi, \\ B_N^{MC}&=\int_0^\pi\int_0^{2\pi}\frac{\partial\rho_1}{\partial\theta}\frac{dP_n^m}{d\theta}P_N^M\sin\theta\sin m\phi\cos M\phi d\theta d\phi, \\ C_N^{MC}&=m\int_0^\pi\int_0^{2\pi}\frac{\partial\rho_1}{\partial\phi}\frac{P_n^mP_N^M}{\sin\theta}\sin m\phi\cos M\phi d\theta d\phi, \\ D_N^{MC}&=m\int_0^\pi\int_0^{2\pi}\frac{\partial\rho_1}{\partial\phi}\frac{P_n^mP_N^M}{\sin\theta}\cos m\phi\cos M\phi d\theta d\phi, \\ E_N^{MC}&=n(n+1)\int_0^\pi\int_0^{2\pi}\rho_1P_n^mP_N^M\sin\theta\cos m\phi\cos M\phi d\theta d\phi, \\ F_N^{MC}&=n(n+1)\int_0^\pi\int_0^{2\pi}\rho_1P_n^mP_N^M\sin\theta\sin m\phi\cos M\phi d\theta d\phi. \end{aligned}\right\} \tag{38}$$

Similarly, the multiplying operation by $P_N^M\sin\theta\sin M\phi$ leads to

$$\sum_n\sum_m[(A_N^{MS}-C_N^{MS}-E_N^{MS})K_n^{mC}+(B_N^{MS}+D_N^{MS}-F_N^{MS})K_n^{mS}]$$
$$=\begin{cases} \beta\left[aNe_N^M\sin\epsilon_N^M\dfrac{2\pi}{2N+1}\dfrac{(N+M)!}{(N-M)!}+8\pi^2\dfrac{N(N+1)}{(2N+1)^2}\dfrac{(N+M)!}{(N-M)!}K_N^{MS}\right] \\ \qquad \text{for } k=N, \quad l=M \\ 8\beta\pi^2\dfrac{N(N+1)}{(2N+1)^2}\dfrac{(N+M)!}{(N-M)!}K_N^{MS} \\ \qquad \text{for other combinations of } N \text{ and } M, \end{cases} \tag{39}$$

where

$$\left.\begin{aligned}
A_N^{MS}&=\int_0^{\pi}\int_0^{2\pi}\frac{\partial\rho_1}{\partial\theta}\frac{dP_n^m}{d\theta}P_N^M\sin\theta\cos m\phi\sin M\phi d\theta d\phi,\\
B_N^{MS}&=\int_0^{\pi}\int_0^{2\pi}\frac{\partial\rho_1}{\partial\theta}\frac{dP_n^m}{d\theta}P_N^M\sin\theta\sin m\phi\sin M\phi d\theta d\phi,\\
C_N^{MS}&=m\int_0^{\pi}\int_0^{2\pi}\frac{\partial\rho_1}{\partial\phi}\frac{P_n^mP_N^M}{\sin\theta}\sin m\phi\sin M\phi d\theta d\phi,\\
D_N^{MS}&=m\int_0^{\pi}\int_0^{2\pi}\frac{\partial\rho_1}{\partial\phi}\frac{P_n^mP_N^M}{\sin\theta}\cos m\phi\sin M\phi d\theta d\phi,\\
E_N^{MS}&=n(n+1)\int_0^{\pi}\int_0^{2\pi}\rho_1P_n^mP_N^M\sin\theta\cos m\phi\sin M\phi d\theta d\phi,\\
F_N^{MS}&=n(n+1)\int_0^{\pi}\int_0^{2\pi}\rho_1P_n^mP_N^M\sin\theta\sin m\phi\sin M\phi d\theta d\phi.
\end{aligned}\right\}\tag{40}$$

Putting $N=1$, $M=0$; $N=1$, $M=1$; $N=2$, $M=0$; ---, (37) and (40) provide a set of simultaneous equations solving which $K_n^{mC}$'s and $K_n^{mS}$'s may be determined.

*1-1. Periodic variation*

When the inducing field is purely periodic, we put

$$p=i\alpha,\ (\alpha=2\pi/T,\ i=\sqrt{-1})\tag{41}$$

where $T$ is the period. In such a case, let us also put

$$\left.\begin{aligned}
K_n^{mC}&=\overline{K}_n^{mC}+iK_n^{mC}*,\\
K_n^{mS}&=\overline{K}_n^{mS}+iK_n^{mS}*.
\end{aligned}\right\}\tag{42}$$

Introducing (42) into (37) and (39), we obtain

$$\begin{aligned}
&\sum_n\sum_m[(A_N^{MC}-C_N^{MC}-E_N^{MC})\overline{K}_n^{mC}+(B_N^{MC}+D_N^{MC}-F_N^{MC})\overline{K}_n^{mS}]\\
&\quad=-8\beta^*\pi^2\frac{N(N+1)}{(2N+1)^2}\frac{(N+M)\,!}{(N-M)\,!}K_N^{MC}*,
\end{aligned}\tag{43}$$

$$\begin{aligned}
&\sum_n\sum_m[(A_N^{MC}-C_N^{MC}-E_N^{MC})K_n^{mC}*+(B_N^{MC}+D_N^{MC}-F_N^{MC})K_n^{mS}*]\\
&=\begin{cases}
-\beta^*\left[aNe_N^M\cos\epsilon_N^M\dfrac{2\pi}{2N+1}\dfrac{(N+M)\,!}{(N-M)\,!}-8\pi^2\dfrac{N(N+1)}{(2N+1)^2}\dfrac{(N+M)\,!}{(N-M)\,!}\overline{K}_N^{MC}\right]\\
\qquad\text{for } k=N,\ l=M\\
8\beta^*\pi^2\dfrac{N(N+1)}{(2N+1)^2}\dfrac{(N+M)\,!}{(N-M)\,!}\overline{K}_N^{MC}\\
\qquad\text{for other combinations of } k \text{ and } l,
\end{cases}
\end{aligned}\tag{44}$$

$$\sum_n \sum_m [(A_N^{MS} - C_N^{MS} - E_N^{MS})\overline{K}_n^{mC} + (B_N^{MS} + D_N^{MS} - F_N^{MS})\overline{K}_n^{mS}]$$
$$= -8\beta^*\pi^2 \frac{N(N+1)}{(2N+1)^2} \frac{(N+M)!}{(N-M)!} K_N^{MS*}, \tag{45}$$

$$\sum_n \sum_m [(A_N^{MS} - C_N^{MS} - E_N^{MS})K_n^{mC*} + (B_N^{MS} + D_N^{MS} - F_N^{MS})K_n^{mS*}]$$
$$= \begin{cases} \beta^*\left[ aNe_N^M \sin \epsilon_N^M \frac{2\pi}{2N+1} \frac{(N+M)!}{(N-M)!} + 8\pi^2 \frac{N(N+1)}{(2N+1)^2} \frac{(N+M)!}{(N-M)!} \overline{K}_N^{MS} \right] \\ \qquad \text{for } k=N,\ l=M \\ 8\beta^*\pi^2 \frac{N(N+1)}{(2N+1)^2} \frac{(N+M)!}{(N-M)!} \overline{K}_N^{MS} \\ \qquad \text{for other combinations of } k \text{ and } l, \end{cases} \tag{46}$$

where

$$\beta^* = a\alpha/\rho_0. \tag{47}$$

(43), (44), (45) and (46) provide a set of simultaneous equations solving which we may determine $\overline{K}_n^{mC}$'s, $K_n^{mC*}$'s, $\overline{K}_n^{mS}$'s, and $K_n^{mS*}$'s.

*1-1-1. Induction by a rotating inducing field*

Rikitake[7),8),9)] advanced a theory of electromagnetic induction within a hemispherical shell, an idealized ocean, by an *Sq* which depends on local time only. Such an induction is equivalent to the one by an inducing field rotating about the earth's axis of rotation. Ashour and Price[23)] also studied an induction problem by a rotating field. In the hope of examining the induction by the *Sq* within a land-sea model, a theory of induction by a rotating inducing field will be formulated in the following.

Assuming that the inducing field solely depends on local time $\tau$, a typical inducing potential is given as

$$W_e = a(r/a)^k (e_{k,c}^l \cos \alpha\tau + e_{k,s}^l \sin \alpha\tau) P_k^l(\cos\theta), \tag{48}$$

where $\alpha$ is the angular measure of time. If the time on the $\phi=0$ meridian is denoted by $t$, a relation

$$\alpha\tau = \alpha t + \phi \tag{49}$$

should hold. The complex form of (48) then reduces to

$$W_e = a(r/a)^k (e_{k,c}^l - ie_{k,s}^l) e^{il(\alpha t+\phi)} P_k^l(\cos\theta), \tag{50}$$

23) A. A. ASHOUR and A. T. PRICE, *Geophys. J.*, **10** (1965), 1-15.

which is also rewritten as

$$W_e=a(r/a)^k[e^l_{k,c}\cos l\phi-e^l_{k,s}\cos(l\phi+\pi/2)$$
$$-i\{e^l_{k,c}\cos(l\phi+\pi/2)+e^l_{k,s}\cos l\phi\}]P^l_k(\cos\theta)e^{ilat}. \tag{51}$$

On comparing (51) to (30), it is apparent that the inducing field is given by the sum of four real and imaginary fields provided proper choice of $e^l_k$ and $\epsilon^l_k$ are made. Accordingly the induced field is readily obtained by applying what we learned in the preceding section to the four fields. Actual application of the theory to an *Sq* will appear in a later section.

*1-2. Aperiodic variation*

In a similar fashion to the theory of electromagnetic induction within a plane sheet, a method for approximately solving an induction in a non-uniform spherical sheet is developed in the following.

Going back to (37), its difference form is written as

$$\sum_n\sum_m[(A^{MC}_N-C^{MC}_N-E^{MC}_N)K^{mC}_n(t)+(B^{MC}_N+D^{MC}_N-F^{MC}_N)K^{mS}_n(t)]$$
$$=\begin{cases}-\gamma[aN\{e^M_N(t+\Delta t)-e^M_N(t)\}\cos\epsilon^M_N\dfrac{2\pi}{2N+1}\dfrac{(N+M)!}{(N-M)!}\\ -8\pi^2\dfrac{N(N+1)}{(2N+1)^2}\dfrac{(N+M)!}{(N-M)!}\{K^{MC}_N(t+\Delta t)-K^{MC}_N(t)\}] & \text{for } k=N,\ l=M\\ 8\gamma\pi^2\dfrac{N(N+1)}{(2N+1)^2}\dfrac{(N+M)!}{(N-M)!}\{K^{MC}_N(t+\Delta t)-K^{MC}_N(t)\} & \\ \qquad\text{for other combinations of } N \text{ and } M,\end{cases} \tag{52}$$

where

$$\gamma=a/\rho_0\Delta t. \tag{53}$$

(52) can be rewritten as

$$K^{MC}_N(t+\Delta t)=K^{MC}_N(t)+\frac{1}{8\gamma\pi^2}\frac{(2N+1)^2}{N(N+1)}\frac{(N-M)!}{(N+M)!}\cdot$$
$$\sum_n\sum_m[(A^{MC}_N-C^{MC}_N-E^{MC}_N)K^{mC}_n(t)+(B^{MC}_N+D^{MC}_N-F^{MC}_N)K^{mS}_n(t)]$$
$$+\lambda\frac{a}{4\pi}\frac{2N+1}{N+1}\{e^M_N(t+\Delta t)-e^M_N(t)\}\cos\epsilon^M_N, \tag{54}$$

in which

Table 4. Dimensionless

| Colatitude \ Longitude | 0° | 15 | 30 | 45 | 60 | 75 | 90 | 105 | 120 | 135 |
|---|---|---|---|---|---|---|---|---|---|---|
| 0° | 0.0005 | 0.0005 | 0.0005 | 0.0005 | 0.0005 | 0.0005 | 0.0005 | 0.0005 | 0.0005 | 0.0005 |
| 15 | 0.0009 | 0.0026 | 0.0137 | 0.0137 | 0.0228 | 0.0137 | 0.0342 | 1.0000 | 0.0137 | 0.0171 |
| 30 | 0.0098 | 1.0000 | 0.0684 | 1.0000 | 1.0000 | 1.0000 | 1.0000 | 1.0000 | 1.0000 | 1.0000 |
| 45 | 0.0068 | 0.0684 | 0.0062 | 0.0684 | 0.0684 | 1.0000 | 1.0000 | 1.0000 | 1.0000 | 0.0062 |
| 60 | 1.0000 | 0.0342 | 0.0068 | 0.0684 | 1.0000 | 1.0000 | 1.0000 | 1.0000 | 0.0684 | 0.0011 |
| 75 | 1.0000 | 1.0000 | 1.0000 | 0.0068 | 0.0008 | 0.0062 | 0.0017 | 1.0000 | 0.0017 | 0.0007 |
| 90 | 0.0011 | 1.0000 | 1.0000 | 0.0011 | 0.0007 | 0.0008 | 0.0007 | 0.0228 | 0.0023 | 0.0013 |
| 105 | 0.0005 | 0.0068 | 1.0000 | 0.0023 | 0.0013 | 0.0007 | 0.0008 | 0.0007 | 0.0016 | 0.0342 |
| 120 | 0.0009 | 0.0017 | 0.0024 | 0.0009 | 0.0005 | 0.0009 | 0.0009 | 0.0007 | 1.0000 | 1.0000 |
| 135 | 0.0007 | 0.0005 | 0.0005 | 0.0006 | 0.0006 | 0.0010 | 0.0014 | 0.0007 | 0.0007 | 0.0006 |
| 150 | 0.0005 | 0.0005 | 0.0005 | 0.0009 | 0.0005 | 0.0012 | 0.0007 | 0.0007 | 0.0006 | 0.0006 |
| 165 | 1.0000 | 1.0000 | 1.0000 | 1.0000 | 1.0000 | 1.0000 | 1.0000 | 1.0000 | 1.0000 | 1.0000 |
| 180 | 1.0000 | 1.0000 | 1.0000 | 1.0000 | 1.0000 | 1.0000 | 1.0000 | 1.0000 | 1.0000 | 1.0000 |

$$\left.\begin{aligned}&\lambda=1 \text{ for } k=N,\ l=M,\\&\lambda=0 \text{ for other combinations of } N \text{ and } M.\end{aligned}\right\} \tag{55}$$

Similarly, the following holds:

$$\begin{aligned}K_N^{MS}(t+\Delta t)=K_N^{MS}(t)+&\frac{1}{8\gamma\pi^2}\frac{(2N+1)^2}{N(N+1)}\frac{(N-M)\,!}{(N+M)\,!}\cdot\\&+\sum_n\sum_m\left[(A_N^{MS}-C_N^{MS}-E_N^{MS})K_n^{mC}(t)+(B_N^{MS}+D_N^{MS}-F_N^{MS})K_n^{mS}(t)\right]\\&-\lambda\frac{a}{4\pi}\frac{2N+1}{N+1}\{e_N^M(t+\Delta t)-e_N^M(t)\}\sin\epsilon_N^M.\end{aligned} \tag{56}$$

It is therefore possible to estimate the coefficients of current function at $t+\Delta t$ from those at $t$ on condition that $\Delta t$ is sufficiently small. The accuracy of the present method may be discussed in a fashion similar to what the writer described in the case of non-uniform plane sheet.

## 2. Application of the theory

It is intended to apply the theory to electromagnetic induction in a non-uniform spherical sheet having any distribution of electric conduc-

resistance $\rho_1$.

| 150 | 165 | 180 | 195 | 210 | 225 | 240 | 255 | 270 | 285 | 300 | 315 | 330 | 345 |
|---|---|---|---|---|---|---|---|---|---|---|---|---|---|
| 0.0005 | 0.0005 | 0.0005 | 0.0005 | 0.0005 | 0.0005 | 0.0005 | 0.0005 | 0.0005 | 0.0005 | 0.0005 | 0.0005 | 0.0005 | 0.0005 |
| 0.0171 | 0.0137 | 0.0053 | 0.0027 | 0.0008 | 0.0010 | 0.0034 | 0.0062 | 0.0114 | 0.0027 | 0.0046 | 1.0000 | 1.0000 | 0.0027 |
| 0.0684 | 0.0085 | 0.0016 | 0.0228 | 0.0062 | 0.0684 | 1.0000 | 1.0000 | 0.0137 | 0.0684 | 0.0020 | 0.0026 | 0.0017 | 0.0017 |
| 0.0011 | 0.0005 | 0.0005 | 0.0005 | 0.0007 | 0.0007 | 1.0000 | 1.0000 | 0.0684 | 1.0000 | 0.0022 | 0.0009 | 0.0011 | 0.0006 |
| 0.0005 | 0.0005 | 0.0006 | 0.0005 | 0.0005 | 0.0006 | 0.0008 | 1.0000 | 0.0062 | 0.0008 | 0.0005 | 0.0009 | 0.0006 | 0.0011 |
| 0.0005 | 0.0009 | 0.0006 | 0.0006 | 0.0005 | 0.0005 | 0.0007 | 0.0010 | 0.0027 | 0.0011 | 0.0008 | 0.0010 | 0.0006 | 0.0068 |
| 0.0010 | 0.0007 | 0.0007 | 0.0007 | 0.0006 | 0.0007 | 0.0007 | 0.0011 | 0.0017 | 1.0000 | 1.0000 | 0.0016 | 0.0007 | 0.0007 |
| 0.0011 | 0.0009 | 0.0015 | 0.0007 | 0.0008 | 0.0008 | 0.0010 | 0.0007 | 0.0007 | 0.0015 | 1.0000 | 1.0000 | 0.0006 | 0.0009 |
| 0.0068 | 0.0011 | 0.0008 | 0.0005 | 0.0006 | 0.0007 | 0.0010 | 0.0014 | 0.0007 | 0.0009 | 1.0000 | 0.0012 | 0.0010 | 0.0012 |
| 0.0007 | 0.0010 | 0.0016 | 0.0006 | 0.0005 | 0.0005 | 0.0007 | 0.0008 | 0.0006 | 0.0040 | 0.0018 | 0.0005 | 0.0006 | 0.0009 |
| 0.0008 | 0.0006 | 0.0006 | 0.0007 | 0.0008 | 0.0007 | 0.0006 | 0.0005 | 0.0005 | 0.0006 | 0.0011 | 0.0017 | 0.0011 | 0.0006 |
| 1.0000 | 0.0027 | 0.0027 | 0.0014 | 0.0006 | 0.0137 | 1.0000 | 1.0000 | 1.0000 | 1.0000 | 1.0000 | 0.0027 | 0.0023 | 1.0000 |
| 1.0000 | 1.0000 | 1.0000 | 1.0000 | 1.0000 | 1.0000 | 1.0000 | 1.0000 | 1.0000 | 1.0000 | 1.0000 | 1.0000 | 1.0000 | 1.0000 |

tivity or resistance. A method of numerical calculation will hence be advanced in this section.

*2-1. Resistance distribution*

A computer programme is compiled in such a way as to read the resistance values at intersection points of meridians and parallel circles. Denoting resistance at a point specified by the $j$-th meridian and $i$-th parallel circle by $\rho_{i,j}$, its derivatives in the $\theta$- and $\phi$-directions are computed by the following formulas:

$$\left.\begin{aligned}\left(\frac{\partial\rho}{\partial\theta}\right)_{i,j}&=\frac{1}{\Delta\theta}\left[\frac{\rho_{i+1,j}-\rho_{i-1,j}}{2}-\frac{1}{6}\,\frac{\rho_{i+2,j}-2\rho_{i+1,j}+2\rho_{i-1,j}-\rho_{i-2,j}}{2}\right],\\ \left(\frac{\partial\rho}{\partial\phi}\right)_{i,j}&=\frac{1}{\Delta\phi}\left[\frac{\rho_{i,j+1}-\rho_{i,j-1}}{2}-\frac{1}{6}\,\frac{\rho_{i,j+2}-2\rho_{i,j+1}+2\rho_{i,j-1}-\rho_{i,j-2}}{2}\right],\end{aligned}\right\}\qquad(57)$$

where $\Delta\theta$ and $\Delta\phi$ are the intervals for reading.

As for the vicinity of singular points, the north and south poles, special caution should be taken for numerically calculating the derivatives. In the immediate neighbourhood of the origin of coordinate systems, which is taken at a pole, we may assume that the curvature is ignored. In that case, referring to Fig. 16, we obtain

$$\left.\begin{aligned}\lim_{r_1\to 0}\frac{\partial\rho}{\partial r_1}&=\left(\frac{\partial\rho}{\partial x}\cos\phi+\frac{\partial\rho}{\partial y}\sin\phi\right)_{r_1=0,}\\ \lim_{r_1\to 0}\frac{\partial\rho}{r_1\partial\phi}&=\left(-\frac{\partial\rho}{\partial x}\sin\phi+\frac{\partial\rho}{\partial y}\cos\phi\right)_{r_1=0.}\end{aligned}\right\}\tag{58}$$

It is therefore possible to calculate from $\partial\rho/\partial x$ and $\partial\rho/\partial y$ at the poles $\partial\rho/\partial\phi$ and $\partial\rho/\partial\theta$ by taking into account $r_1=a\theta$, where $a$ denotes the radius of the spherical sheet. $\partial\rho/\partial x$ and $\partial\rho/\partial y$ may be obtained by making differences between $\rho$'s adjacent to that at the poles. $\partial\rho/\partial\theta$ values on the parallel circles next to the poles may also be calculated from simple differences between $\rho$'s on the next circles and at the poles.

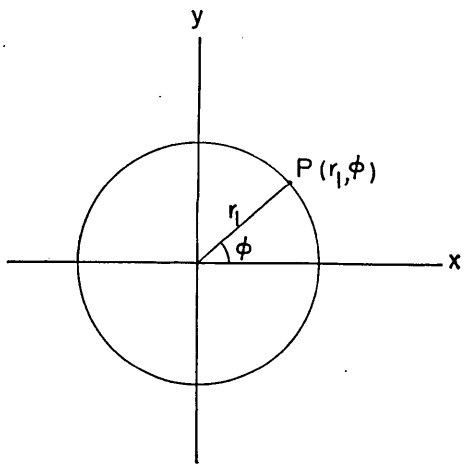

Fig. 16. Coordinate systems.

Although the accuracy of the derivatives at points around the poles is somewhat lower than that computed by (57), it is believed that no serious error would be induced in the estimate of integrals involving $\partial\rho_1/\partial\theta$ and $\partial\rho_1/\partial\phi$ in (38) and (40) because only the end values of integrands are calculated in such a way.

As an example of non-uniform sheet, a hypothetical spherical sheet which seems likely to represent the surface conductivity distribution of the earth is considered. The depths of the sea are read off at intersection points of meridians and parallel circles at 15° interval from a chart published by the U. S. Naval Oceanographic Office[24]. They are then multiplied by specific conductivity of the sea-water, $4\times10^{-11}$ e.m.u. say, and their reciprocals are taken as the resistance of the sheet over the sea area. As for the land area, specific conductivity $10^{-14}$ e.m.u. and thickness 10 km are assumed, so that the resistance over the continental area is assumed as $10^8$ e.m.u. In the actual readings, averaged value around an intersection point is adopted in order to avoid extreme values. The dimensionless resistance $\rho_1$ normalized by taking $\rho_0$ as $10^8$ e.m.u. is given in Table 4. The distribution of $\log_{10}(10^4\,\rho_1)$ is illustrated in Fig. 17. Looking at

24) U. S. NAVAL OCEANOGRAPHIC OFFICE, *Chart of the world, 10th ed.*, (1961).

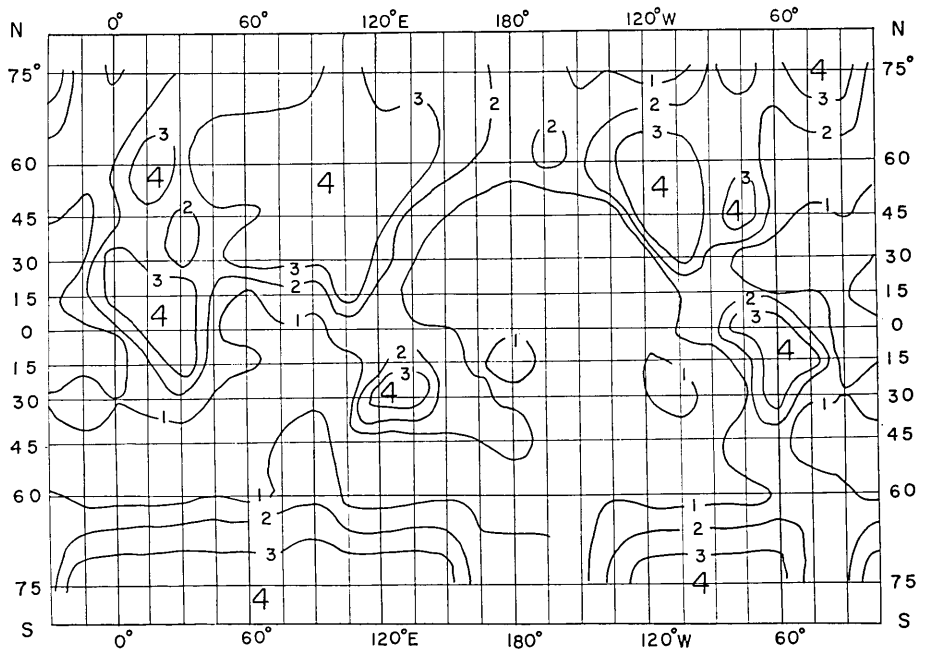


Fig. 17. World's distribution of $\log_{10}(10^4\rho_1)$, where $\rho_1$ is the dimensionless resistance.

Fig. 17, we notice that one of the steepest gradients of the resistance can be seen at the western coast of North America.

Taking the earth's radius as $6.37\times10^8$ cm, we obtain

$$a/\rho_0=6.37 \text{ e.m.u.} \tag{59}$$

Numerical results in the following sections will hold good for any combinations of $a$ and $\rho_0$ as long as they satisfy (59).

*2-2. Computation of the integrals (38) and (40)*

It is first required for solving the induction problem to compute the integrals involved in (38) and (40). For that purpose function subprogrammes for $P_n^m(\cos\theta)$, $\sin\theta dP_n^m/d\theta$ and $P_n^m/\sin\theta$ are compiled. The integrals are then performed by making use of the Filon and Simpson methods which have already been described in Part 1 of this paper. Spherical harmonic functions only up to degree 3 and order 3 are considered in the present work owing to the time-consuming computer work. It is therefore not possible to study local features of induced electric currents or magnetic fields which are to be described by spherical

functions having degrees or orders higher than 3.

*2-3. Simultaneous equations*

Equations from (43) to (46) provide a set of simultaneous equations with 36 equations in the present case. They are solved by the method already described in Subsection 3-3 in Part 1 of this paper.

*2-4. Test solutions*

The whole programme is tested by solving inductions by a uniform magnetic field in a uniform sheet as well as in the Ashour-Price model[5] for which the conductivity is given by

$$\rho_1 = 1 + 0.9 \cos\theta. \tag{60}$$

In the latter case $\rho_0 = 1.636 \times 10^7$ e.m.u., $e_1^1 = 1$ and $a = 6.44 \times 10^8$ cm (the radius of the ionospheric $E$ layer) are assumed following Ashour and Price. For a period of 2 min., the non-vanishing coefficients of current function $K_n^{1C}$'s and $K_n^{1S}$'s are calculated as given in Table 5 in which the values deduced from the Ashour-Price's results are also indicated.

Table 5. Current function coefficients for 2 min. period for the Ashour-Price model.

| $n$ | Present method | | Ashour-Price method | |
|---|---|---|---|---|
| | $\bar{K}_n^{1C}$ | $K_n^{1C*}$ | $\bar{K}_n^{1C}$ | $K_n^{1C*}$ |
| 1 | 0.11730 | 0.01332 | 0.11750 | 0.01352 |
| 2 | −0.00286 | 0.00560 | −0.00093 | 0.00319 |
| 3 | −0.00029 | −0.00027 | −0.00018 | −0.00011 |

It seems to the writer that the agreement between both the results is fairly good in spite of the not very accurate performance of the integrations involved in (38) and (40). The agreement between the present and Ashour-Price's results become slightly bad for longer periods of the inducing field.

*2-5. Examples of induction by periodic inducing fields in the land-sea model*

Electromagnetic induction in a non-uniform spherical sheet, a hypothetical land-sea model given in Subsection 2-1, by a uniform inducing

Table 6 a. Current function coefficients for the land-sea model. $T=1$ min.

| $n$ | $m$ | $\overline{K}_n^{mC}$ | $K_n^{mC*}$ | $\overline{K}_n^{mS}$ | $K_n^{mS*}$ |
|---|---|---|---|---|---|
| 1 | 0 | 0.1172 | 0.0151 | — | — |
| 1 | 1 | 0.0002 | −0.0010 | 0.0007 | −0.0012 |
| 2 | 0 | −0.0019 | 0.0050 | — | — |
| 2 | 1 | −0.0003 | 0.0018 | 0.0003 | −0.0005 |
| 2 | 2 | −0.0001 | 0·0004 | 0.0001 | −0.0005 |
| 3 | 0 | −0.0019 | 0.0022 | — | — |
| 3 | 1 | 0.0000 | 0.0004 | −0.0002 | 0.0005 |
| 3 | 2 | −0.0001 | 0.0000 | 0.0000 | −0.0001 |
| 3 | 3 | 0.0000 | 0.0000 | 0.0000 | 0.0000 |

Table 6 b. Current function coefficients for the land-sea model. $T=1$ hour.

| $n$ | $m$ | $\overline{K}_n^{mC}$ | $K_n^{mC*}$ | $\overline{K}_n^{mS}$ | $K_n^{mS*}$ |
|---|---|---|---|---|---|
| 1 | 0 | 0.0193 | 0.0122 | — | — |
| 1 | 1 | 0.0001 | −0.0019 | −0.0018 | 0.0021 |
| 2 | 0 | −0.0026 | −0.0024 | — | — |
| 2 | 1 | −0.0079 | −0.0007 | 0.0009 | −0.0001 |
| 2 | 2 | −0.0033 | 0.0012 | 0.0024 | 0.0001 |
| 3 | 0 | −0.0003 | −0.0007 | — | — |
| 3 | 1 | −0.0027 | 0.0001 | 0.0001 | −0.0001 |
| 3 | 2 | 0.0001 | −0.0003 | 0.0004 | 0.0003 |
| 3 | 3 | 0.0000 | 0.0000 | 0.0001 | −0.0001 |

Table 6 c. Current function coefficients for the land-sea model. $T=1$ day.

| $n$ | $m$ | $\overline{K}_n^{mC}$ | $K_n^{mC*}$ | $\overline{K}_n^{mS}$ | $K_n^{mS*}$ |
|---|---|---|---|---|---|
| 1 | 0 | 0.0165 | 0.0019 | — | — |
| 1 | 1 | 0.0033 | 0.0001 | −0.0026 | −0.0001 |
| 2 | 0 | −0.0019 | −0.0003 | — | — |
| 2 | 1 | −0.0071 | −0.0006 | 0.0010 | 0.0001 |
| 2 | 2 | −0.0039 | −0.0003 | 0.0022 | 0.0002 |
| 3 | 0 | 0.0001 | 0.0000 | — | — |
| 3 | 1 | −0.0027 | −0.0002 | 0.0001 | 0.0000 |
| 3 | 2 | 0.0012 | 0.0001 | −0.0005 | 0.0000 |
| 3 | 3 | 0.0000 | 0.0000 | 0.0001 | 0.0000 |

field parallel to the earth's rotation axis is examined. Assuming that the inducing field has a unit amplitude and that its period is 1 min, 1 hour, and 1 day, the current function coefficients are computed as indicated in Tables 6 a, 6 b, and 6 c.

The accuracy of the coefficients given in the tables is not known. Judging from the test solutions in the last subsection, however, they seem to be good enough for discussing the gross characteristics of the electric currents induced in the model. In the tables, we in fact observe that the coefficients get generally smaller for higher spherical functions.

In the case of the 1 min. period induction, the coefficients for $n=1$ and $m=0$ are so large that other harmonics can be practically ignored in drawing stream lines of the induced currents. The land-sea model behaves in a fashion very close to a perfect conductor in this case, and so the induced currents flow almost along the parallel circles. If the inducing field taken positive northwards, the induced currents flow from east to west.

For a slower variation, $T=1$ hour say, the intensity of the induced

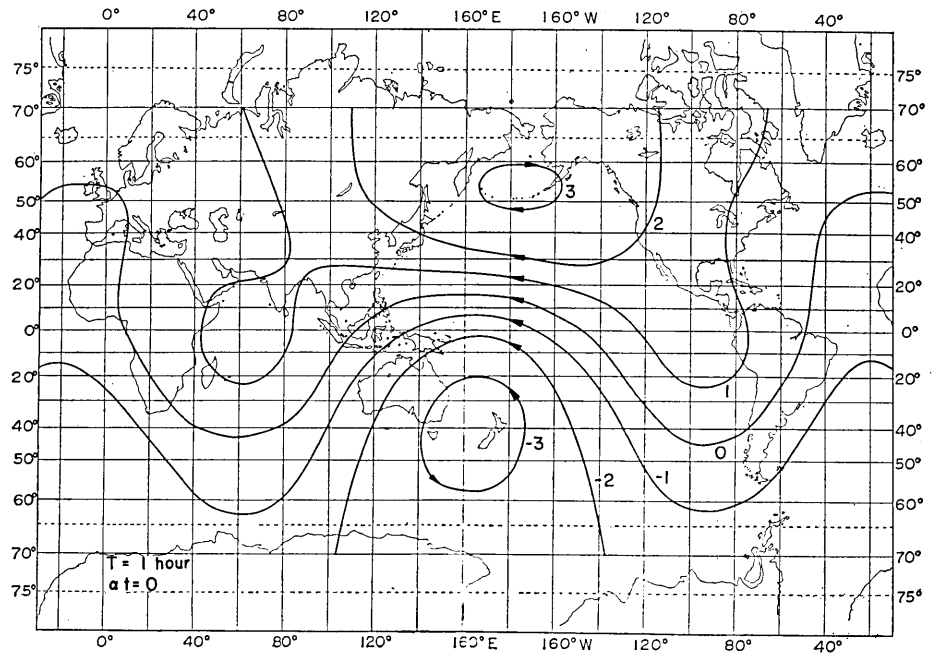


Fig. 18 a. Induced current lines in units of the uniform axial inducing field multiplied by 0.01. $T=1$ hour, $\alpha t=0$.

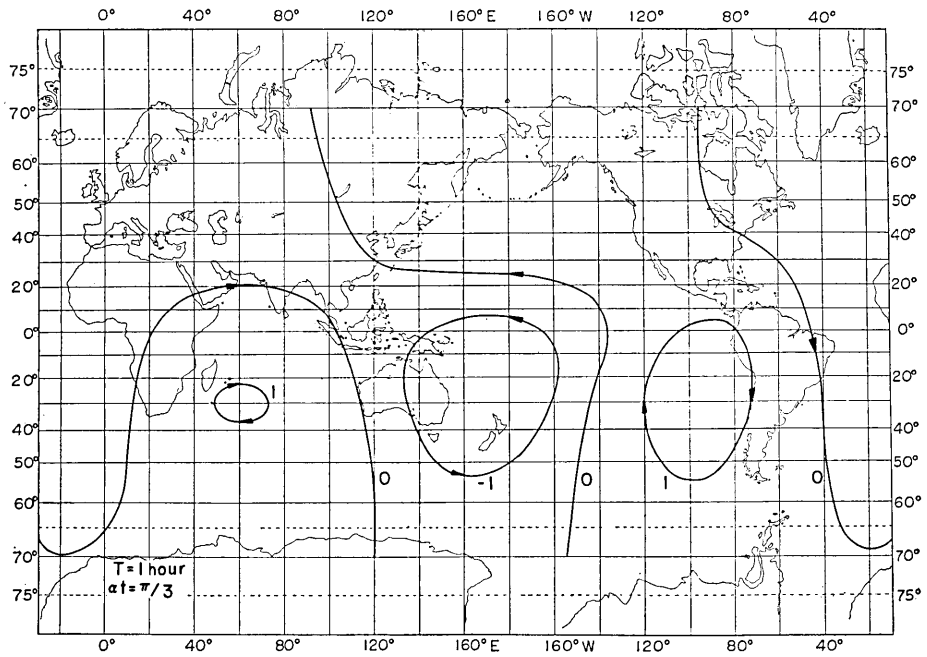


Fig. 18 b. Induced current lines in units of the uniform axial field multiplied by 0.01. $T=1$ hour, $\alpha t=\pi/3$.

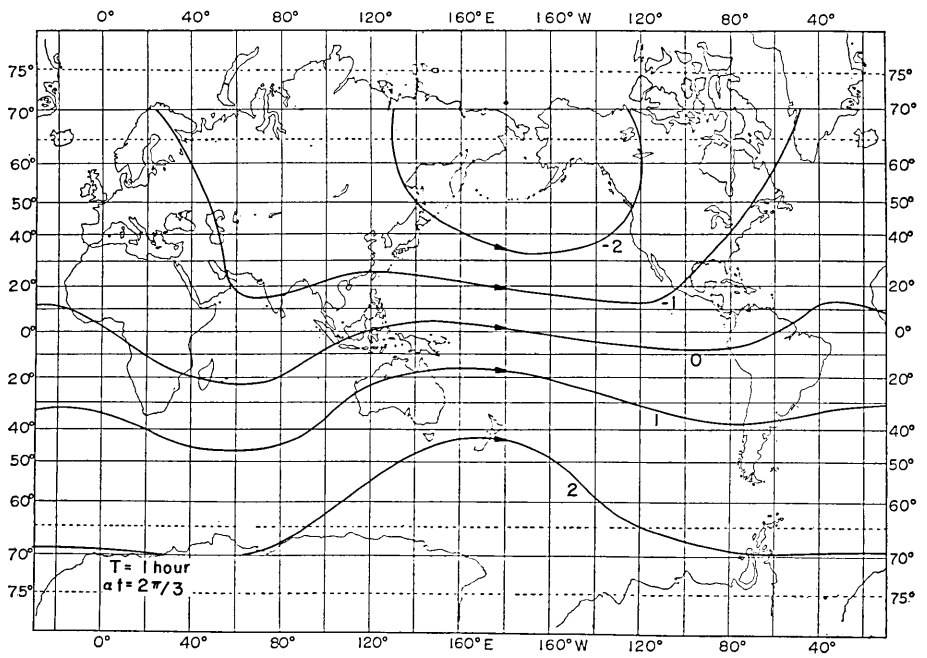


Fig. 18 c. Induced current lines in units of the uniform axial field multiplied by 0.01. $T=1$ hour, $\alpha t=2\pi/3$.

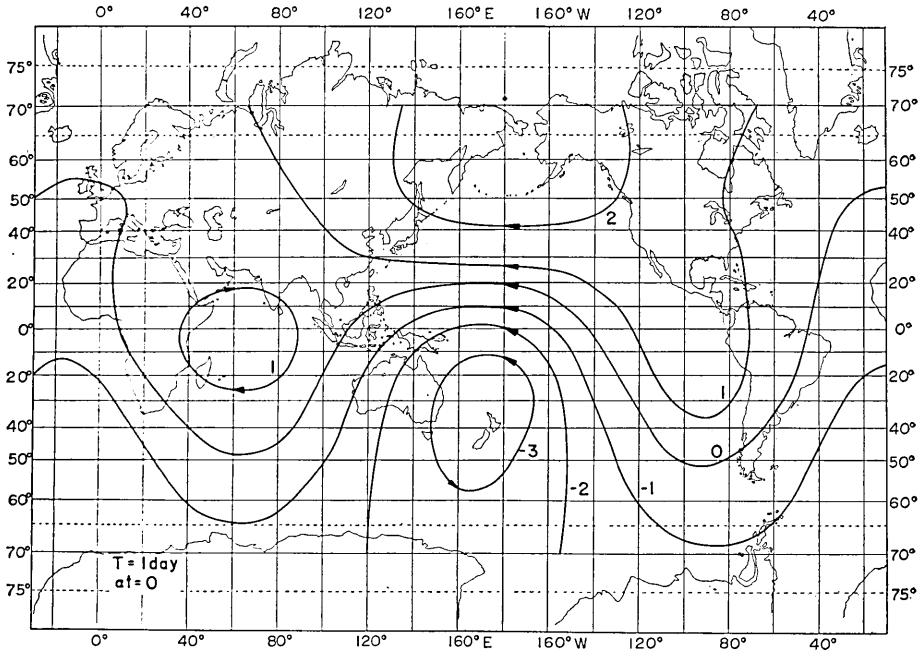


Fig. 19 a. Induced current lines in units of the uniform axial field multiplied by 0.01. $T=1$ day, $\alpha t=0$.

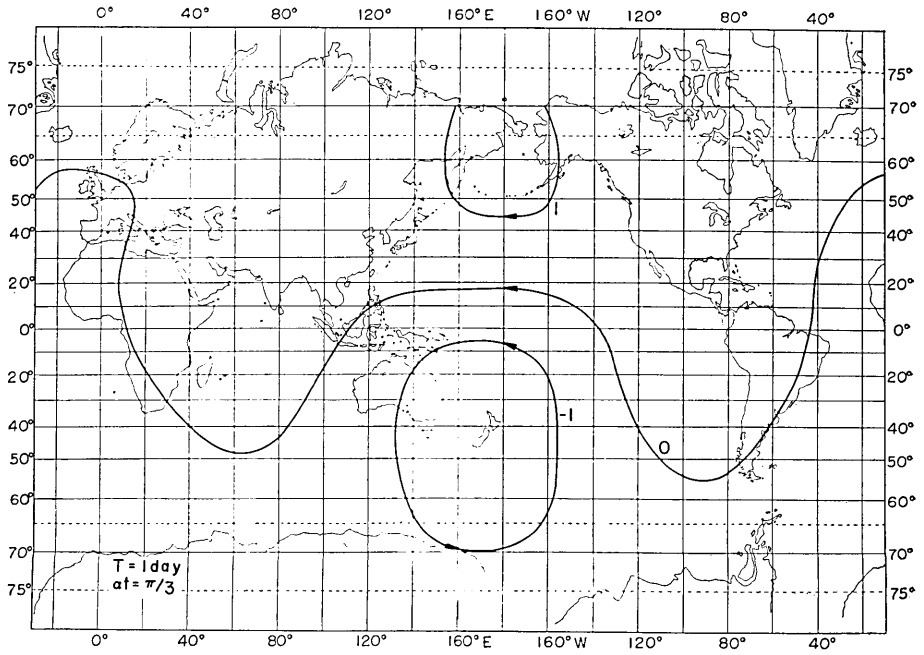


Fig. 19 b. Induced current lines in units of the uniform axial field multiplied by 0.01. $T=1$ day, $\alpha t=\pi/3$.

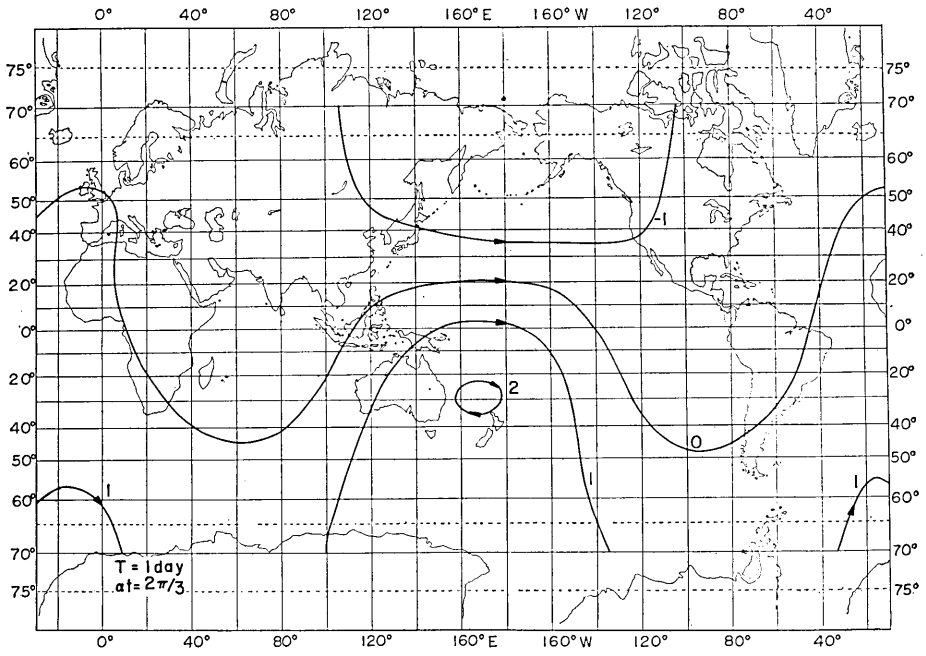


Fig. 19 c. Induced current lines in units of the uniform axial field multiplied by 0.01. $T=1$ day, $\alpha t=2\pi/3$.

current becomes small by one order of magnitude and the pattern of flow tends to deviate from the zonal flow. In Figs. 18 a, 18 b, and 18 c are illustrated the stream lines for $T=1$ hour at epochs $\alpha t=0$, $\pi/3$ and $2\pi/3$. Although the east-west flow of the induced currents are important for most of the time, the deflection of the currents from the high resistance portions of the sheet, that is the Eurasian and American continents, can be clearly observed. On the contrary, the high concentration of the current in the Central Pacific, the encirclings of the current in the South Pacific and Indian Oceans are outstanding. Current circulations, though less remarkable, also occur in the North Pacific and South-east Pacific. The land-sea model seems so crude that the Australian Continent and the Indonesian Islands do not behave as a serious obstacle for the flow of induced currents. It seems likely that spherical harmonic functions having ranks higher than those treated in the present analysis should be taken into account in order to represent the right effect of such features of land-sea distribution.

The magnetic fields produced by the induced currents can also be

readily calculated although no illustrations are given here. The intensity of the field components becomes very high at the centres of current vortices, i.e. the vertical field at 170°E, 35°S and 180°E, 55°N reaches 70—80 per cent of that of the inducing field.

The distribution patterns of the stream lines of the induced electric currents for $T=1$ day prove much the same as those for $T=1$ hour. In Figs. 19 a, 19 b and 19 c are illustrated the stream lines for $T=1$ day at epochs $\alpha t=0$, $\pi/3$ and $2\pi/3$. In this case the current density is a little smaller than that for $T=1$ hour, and so the magnetic fields produced by the currents are somewhat weaker. The positions of the vortex centres are more or less the same as those for $T=1$ hour.

*2-6. Induction by an Sq*

As an example of induction by a magnetic field rotating around the earth, it would be interesting to study the induction by an *Sq*. Probably one of the newest analyses of the *Sq* during the International Geophysical Year (IGY) would be the one made by Matsushita and Maeda[25]. Assuming that only the field constituents expressed by spherical harmonic functions of $n=2$ and $m=1$ and $n=3$ and $m=2$ are important, their analysis leads to the following coefficients of the external potential for the yearly average.

Table 7. Main coefficients in units of gamma of the external part of the magnetic potential of the *Sq*.
(Schmidt spherical functions are used.)

| $n$ | $m$ | $e^m_{n,c}$ | $e^m_{n,s}$ |
|---|---|---|---|
| 2 | 1 | 14.22 | −0.01 |
| 3 | 2 | − 6.61 | 1.41 |

The equi-potential lines of the external part of such an idealized *Sq* at 0 h U. T. are illustrated in Fig. 20.

On the other hand, the computer programme for the periodic induction facilitates us to calculate the current function coefficients of the induced field for the four types of the inducing field as given in (51). In Tables 8 a, 8 b, 8 c, and 8 d are given the coefficients for the inducing potential $P_2^1\cos\phi$, $P_2^1\cos(\phi+\pi/2)$, $P_3^2\cos 2\phi$ and $P_3^2\cos(2\phi+\pi/2)$ each having the

25) S. MATSUSHITA and H. MAEDA, *J. Geophys. Res.*, 70 (1965), 2535-2558.

unit amplitude. The period is 1 day for the first two and 12 hours for the others. The land-sea model defined earlier is also made use of.

Summing up the current functions, of which the coefficients are given in Tables 8 a, 8 b, 8 c, and 8 d, for a specified value of $\alpha t$, it is

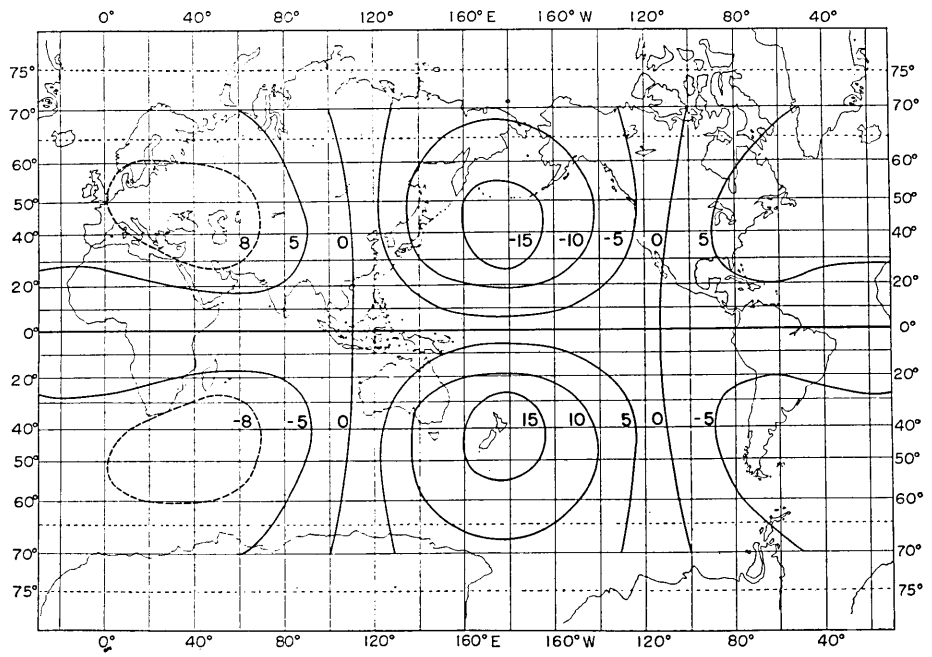


Fig. 20. The external part of the magnetic potential at 0 h U. T. The potential values divided by the earth's radius are given in units of gamma.

Table 8 a. Current function coefficients for $P_2^1 \cos \phi$.

| $n$ | $m$ | $K_n^{mC}$ | $K_n^{mC*}$ | $K_n^{mS}$ | $K_n^{mS*}$ |
|---|---|---|---|---|---|
| 1 | 0 | −0.13037 | −0.01203 | — | — |
| 1 | 1 | −0.02579 | 0.00054 | 0.02021 | 0.00068 |
| 2 | 0 | 0.01476 | 0.00158 | — | — |
| 2 | 1 | 0.05625 | 0.00561 | −0.00775 | −0.00065 |
| 2 | 2 | 0.03059 | 0.00185 | −0.01731 | −0.00129 |
| 3 | 0 | −0.00107 | 0.00052 | — | — |
| 3 | 1 | 0.02123 | 0.00166 | −0.00069 | −0.00004 |
| 3 | 2 | −0.00951 | −0.00068 | 0.00422 | 0.00025 |
| 3 | 3 | 0.00008 | 0.00002 | −0.00081 | −0.00006 |

Table 8 b. Current function coefficients for $P_2^1 \cos(\phi+\pi/2)$.

| $n$ | $m$ | $\overline{K}_n^{mC}$ | $K_n^{mC*}$ | $\overline{K}_n^{mS}$ | $K_n^{mS*}$ |
|---|---|---|---|---|---|
| 1 | 0 | −0.01148 | −0.00077 | — | — |
| 1 | 1 | −0.00224 | 0.00077 | 0.00178 | 0.00038 |
| 2 | 0 | 0.00130 | 0.00020 | — | — |
| 2 | 1 | 0.00495 | 0.00054 | −0.00068 | −0.00047 |
| 2 | 2 | 0.00268 | 0.00010 | −0.00153 | −0.00046 |
| 3 | 0 | −0.00009 | 0.00005 | — | — |
| 3 | 1 | 0.00187 | 0.00015 | −0.00006 | 0.00018 |
| 3 | 2 | −0.00084 | −0.00006 | 0.00037 | 0.00002 |
| 3 | 3 | 0.00001 | 0.00004 | −0.00007 | 0.00002 |

Table. 8 c. Current function coefficients for $P_3^2 \cos 2\phi$.

| $n$ | $m$ | $\overline{K}_n^{mC}$ | $K_n^{mC*}$ | $\overline{K}_n^{mS}$ | $K_n^{mS*}$ |
|---|---|---|---|---|---|
| 1 | 0 | 0.48132 | 0.02791 | — | — |
| 1 | 1 | 0.09514 | −0.00322 | −0.07449 | 0.00281 |
| 2 | 0 | −0.05449 | −0.00171 | — | — |
| 2 | 1 | −0.20760 | −0.00811 | 0.02858 | 0.00068 |
| 2 | 2 | −0.11286 | −0.00254 | 0.06387 | 0.00133 |
| 3 | 0 | 0.00393 | −0.00230 | — | — |
| 3 | 1 | −0.07832 | −0.00204 | 0.00257 | 0.00034 |
| 3 | 2 | 0.03511 | 0.00199 | −0.01557 | −0.00041 |
| 3 | 3 | −0.00028 | 0.00004 | 0.00298 | −0.00001 |

Table 8 d. Current function coefficients for $P_3^2 \cos(2\phi+\pi/2)$.

| $n$ | $m$ | $\overline{K}_n^{mC}$ | $K_n^{mC*}$ | $\overline{K}_n^{mS}$ | $K_n^{mS*}$ |
|---|---|---|---|---|---|
| 1 | 0 | 0.08734 | −0.00043 | — | — |
| 1 | 1 | 0.01762 | 0.00675 | −0.01398 | −0.00918 |
| 2 | 0 | −0.00995 | −0.00108 | — | — |
| 2 | 1 | −0.03765 | 0.00221 | 0.00519 | 0.00014 |
| 2 | 2 | −0.02127 | −0.00050 | 0.01212 | 0.00249 |
| 3 | 0 | 0.00080 | 0.00102 | — | — |
| 3 | 1 | −0.01425 | −0.00024 | 0.00045 | −0.00053 |
| 3 | 2 | 0.00640 | 0.00039 | −0.00286 | −0.00018 |
| 3 | 3 | −0.00006 | −0.00017 | 0.00053 | −0.00002 |

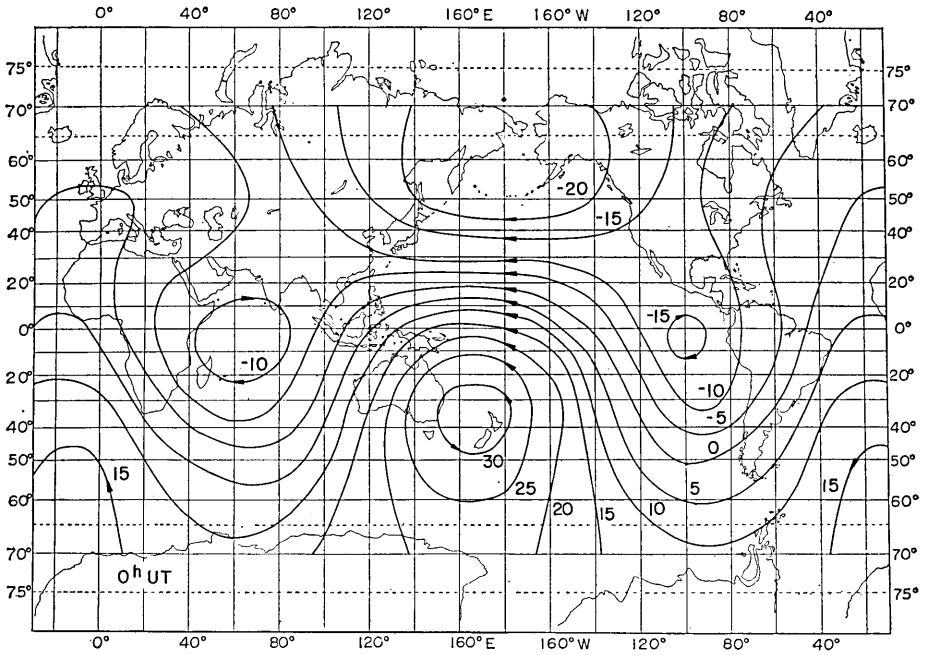


Fig. 21 a. Iuduced current lines in units of $10^{-6}$ e.m.u. for the *Sq* at 0 h U. T.

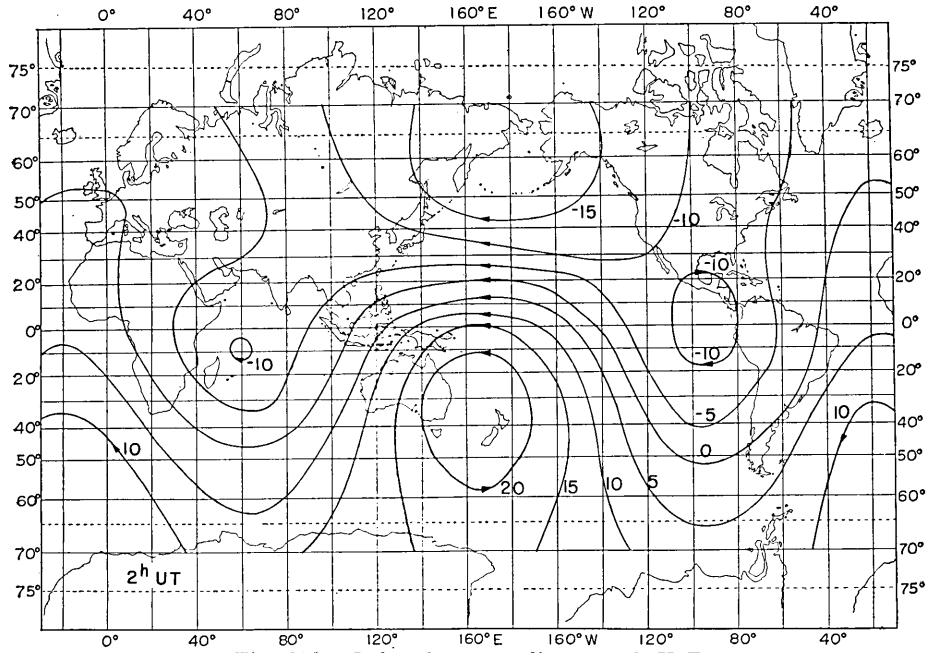


Fig. 21 b. Induced current lines at 2 h U. T.

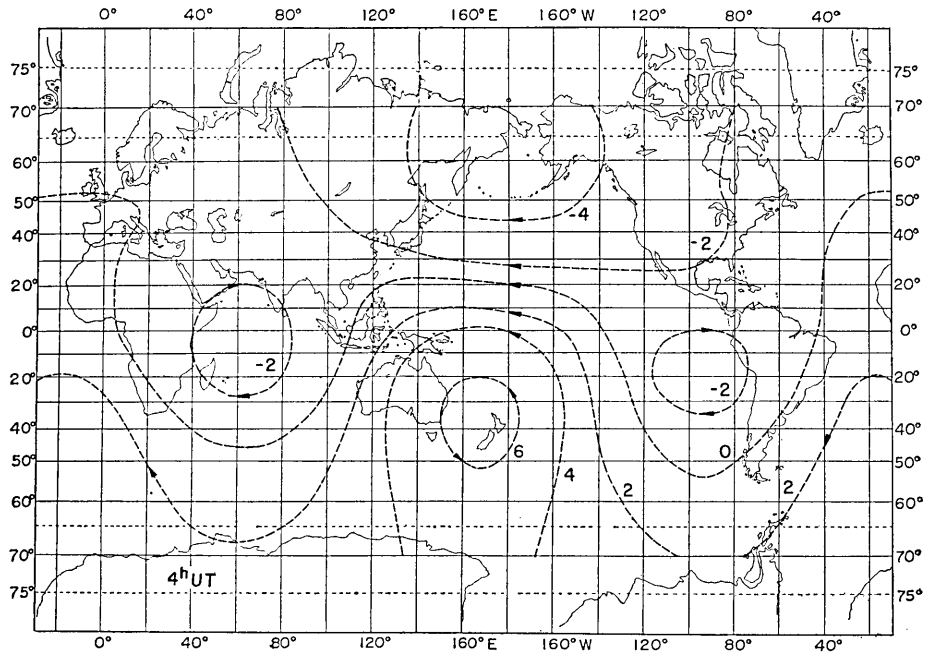


Fig. 21 c. Induced current lines at 4 h U. T.

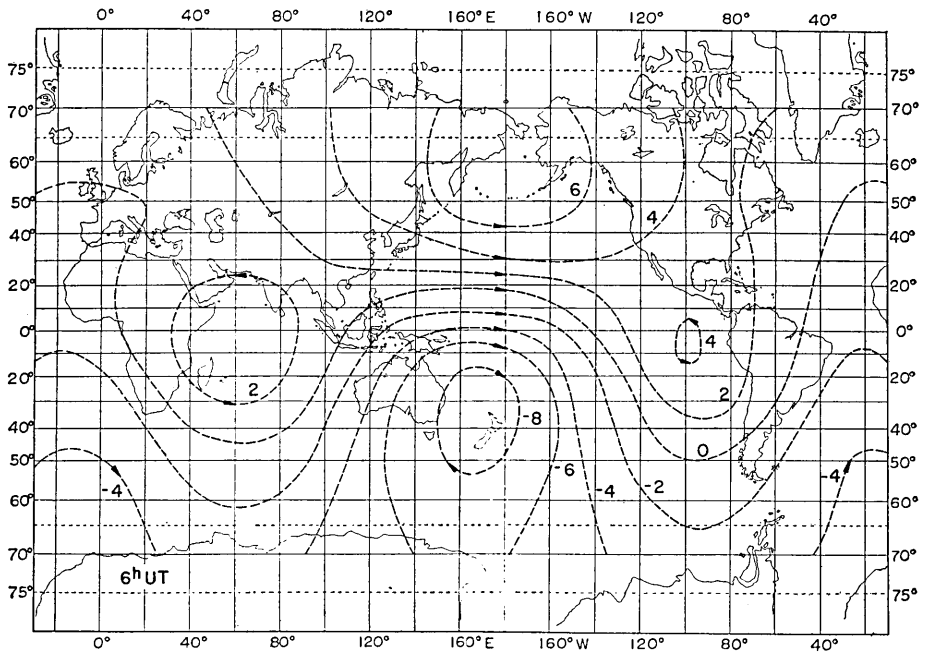


Fig. 21 d. Induced current lines at 6 h U. T.

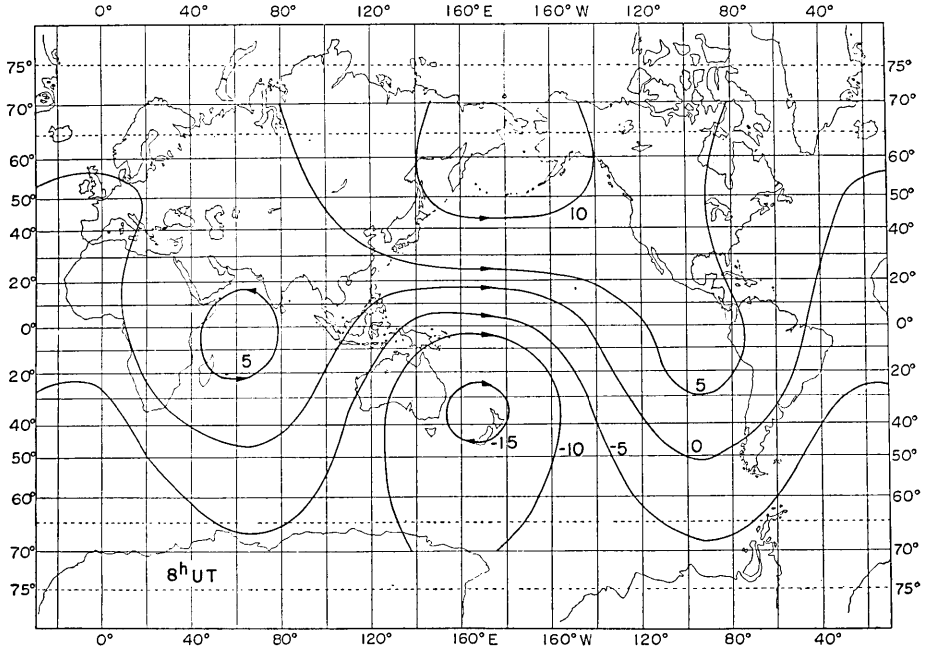


Fig. 21 e. Induced current lines at 8 h U. T.

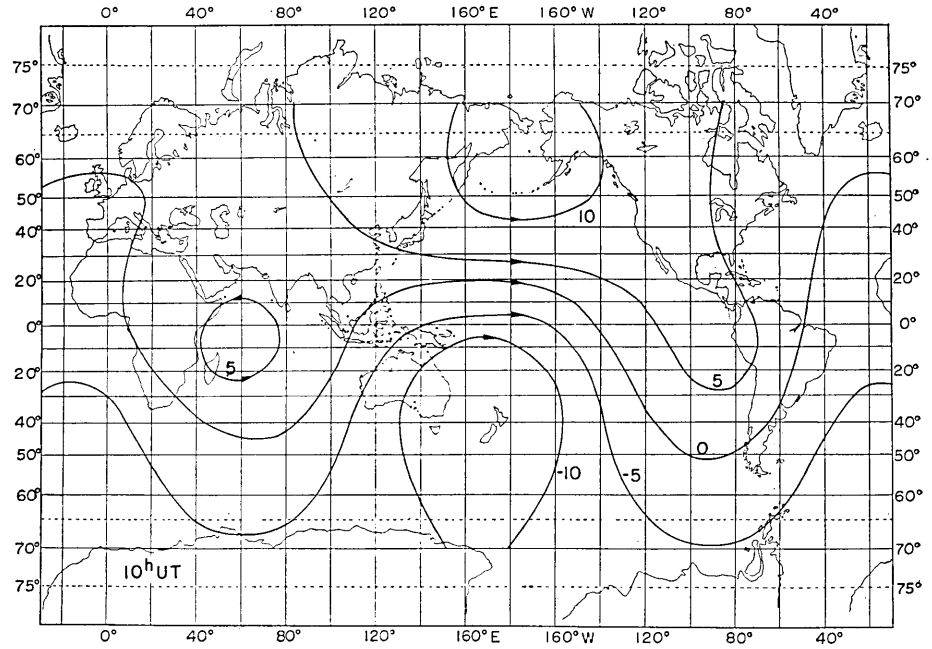


Fig. 21 f. Induced current lines at 10 h U. T.

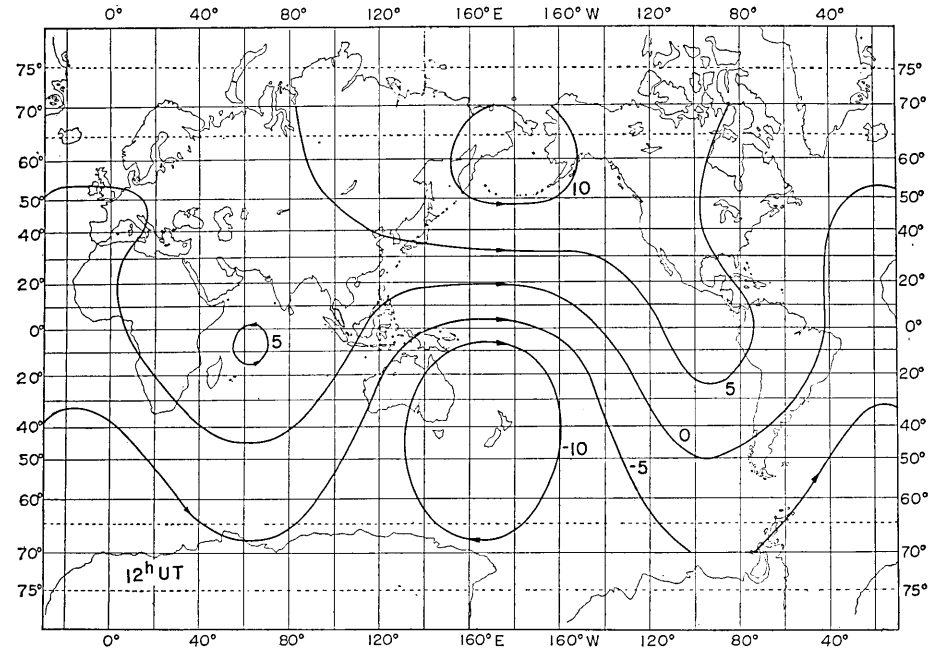


Fig. 21 g. Induced current lines at 12 h U. T.

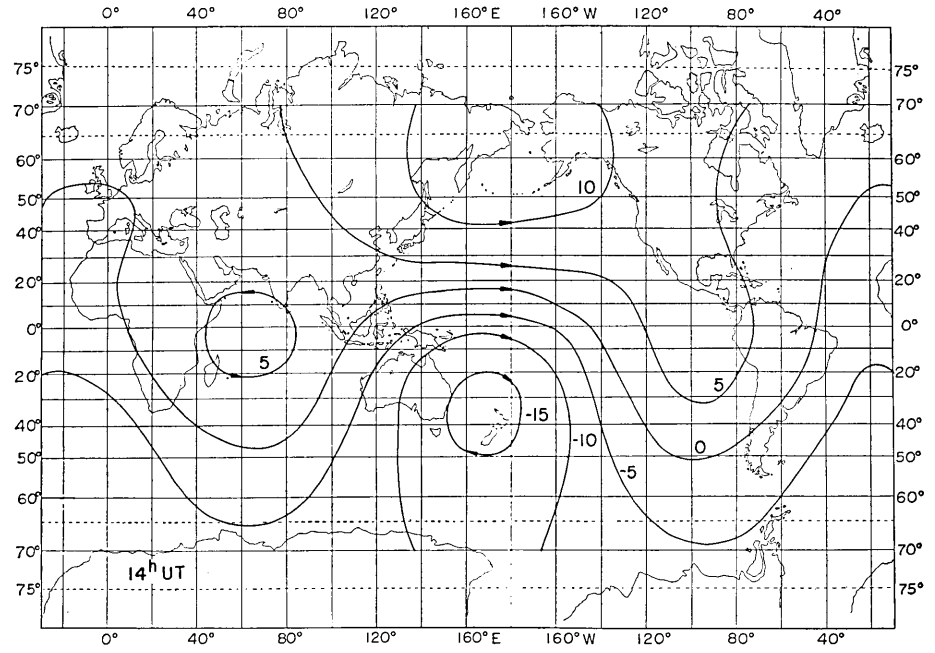


Fig. 21 h. Induced current lines at 14 h U. T.

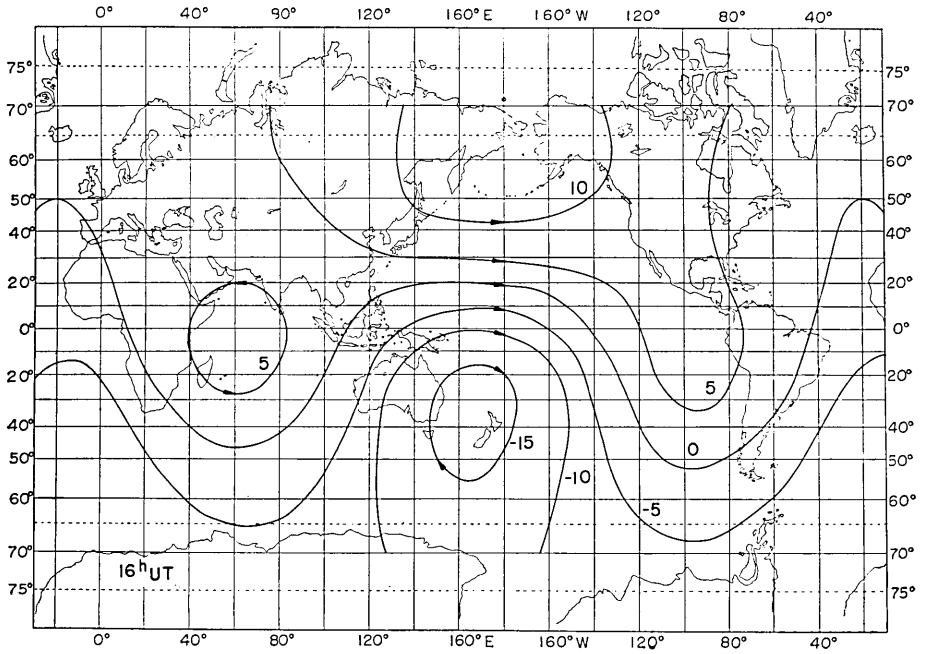


Fig. 21 i. Induced current lines at 16 h U. T.

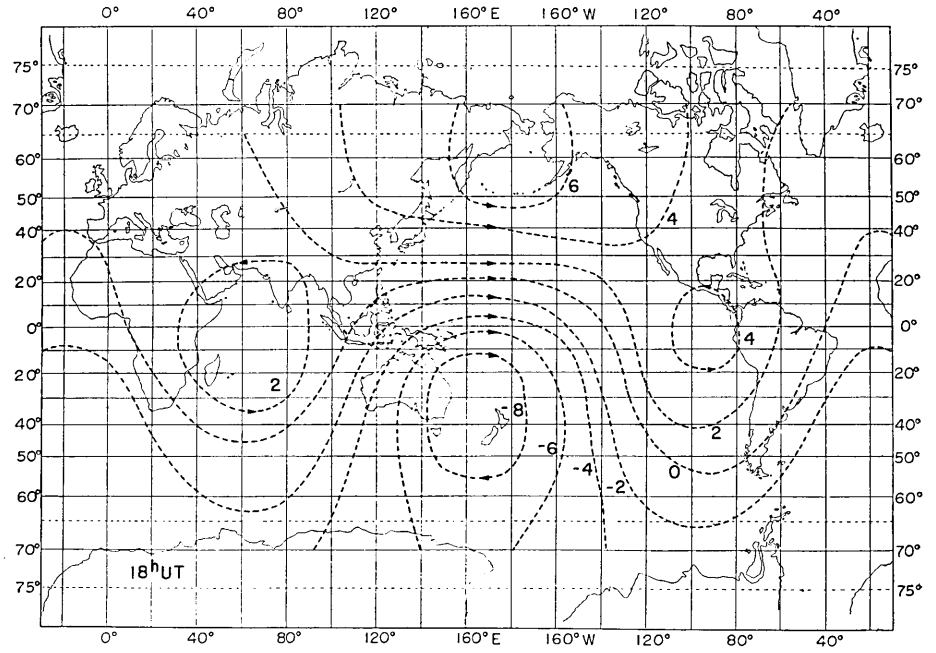


Fig. 21 j. Induced current lines at 18 h U. T.

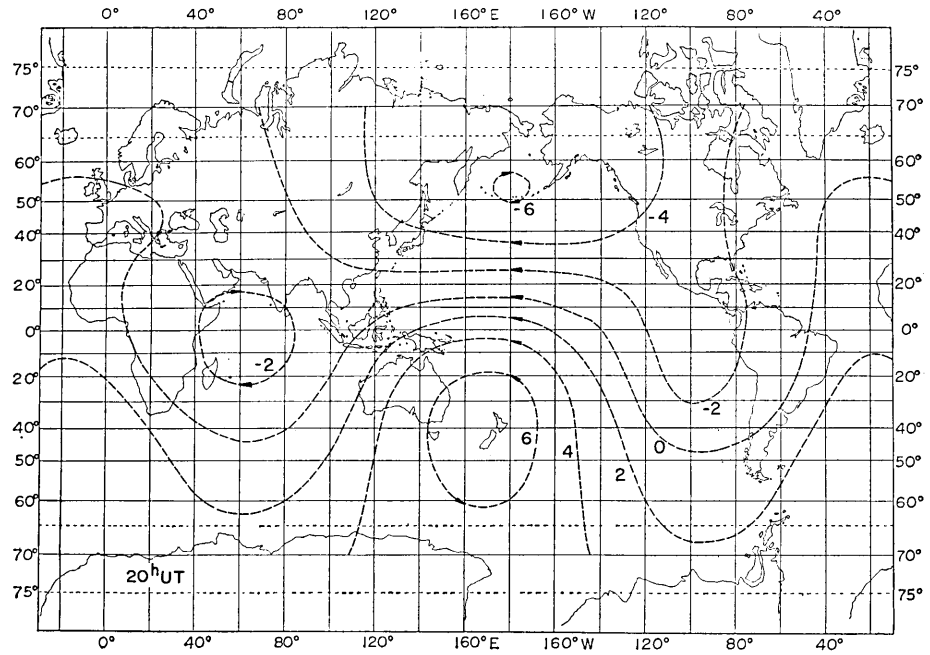


Fig. 21 k. Induced current lines at 20 h U. T.

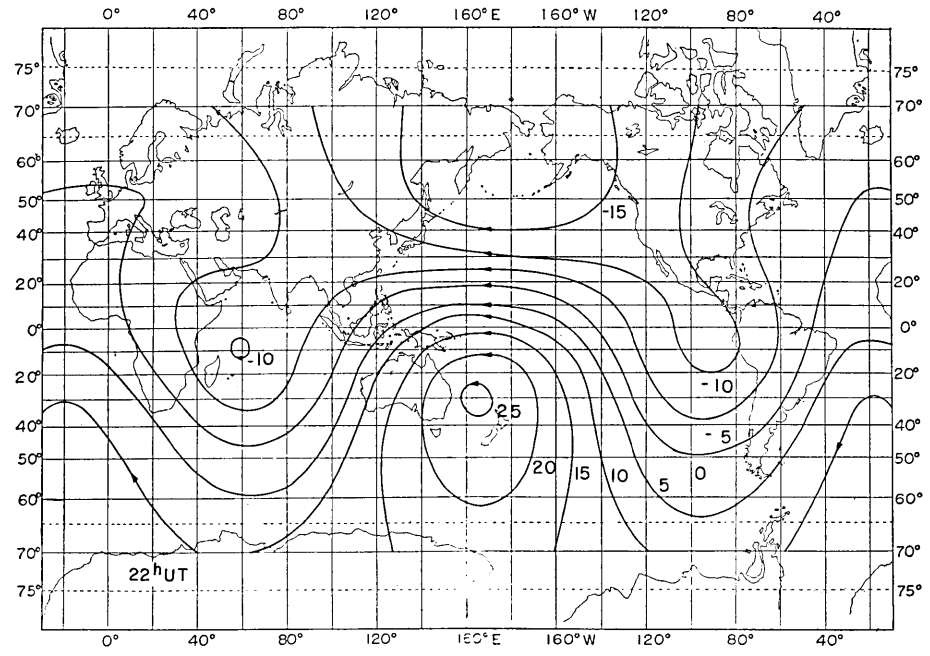


Fig. 21 l. Induced current lines at 22 h U. T.

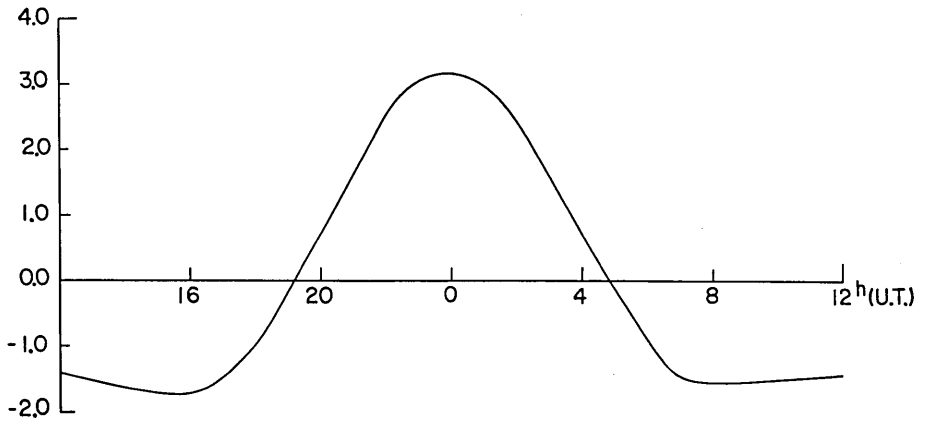


Fig. 22. Change in the current function value in units of $10^{-6}$ e.m.u. at a point defined by 160°E and 30°S.

possible to get at the current lines induced in the land-sea model provided proper account of the real and imaginary parts of the expression is taken.

In the illustrations from Fig. 21 a to Fig. 21 l are shown the induced current patterns for $\alpha t = 0°$, 30°, 60°, 90°, 120°, 150°, 180°, 210°, 240°, 270°, 300°, and 330°. These epochs respectively correspond to 0 h, 2 h, 4 h, 6 h, 8 h, 10 h, 12 h, 14 h, 16 h, 18 h, 20 h, and 22 h in U. T. It is interesting to note that the induced current system is intense around 0 h when the daytime current vortices of external origin are over the Pacific Ocean, that is the most conducting part of the sheet. Meanwhile the intensity becomes weak for epochs around 12 h. Price and Wilkins[26], who analyzed the *Sq* during the 1932-1933 Second International Polar Year, pointed out that the internal potential of the *Sq* becomes very weak and also that the equi-potentials over the southern hemisphere split into two vortices for these epochs. Price and Wilkins suspected that these vortices might be produced by the electric currents induced in the Atlantic and Indian Oceans.

It is not quite clear whether the present results support Price-Wilkins' view because the model does not properly include the high-conducting mantle below a few hundred kilometers from the earth's surface. But it is demonstrated that a fairly intense current vortex is induced in the Indian Ocean. The most intense current vortex appears over the southern Pacific, while less intense ones are seen off the Pacific

26) A. T. PRICE and G. A. WILKINS, *Phil. Trans. Roy. Soc. London*, **256** (1963), 31-98.

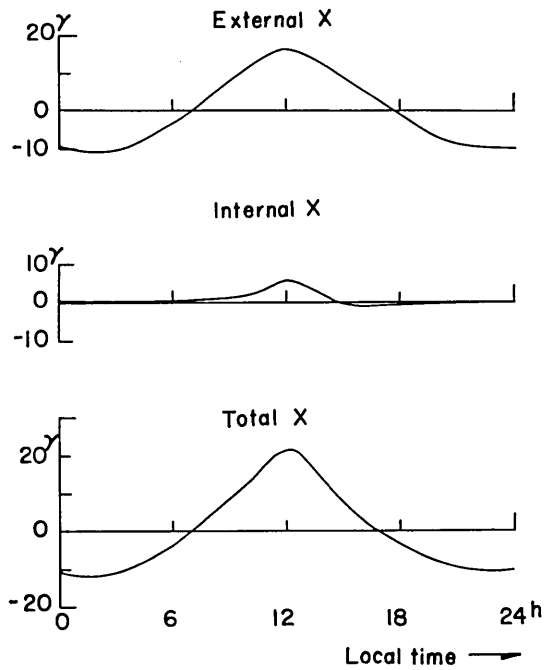


Fig. 23 a. External, internal and total $X$ components of the $Sq$ at 160°E, 30°S.

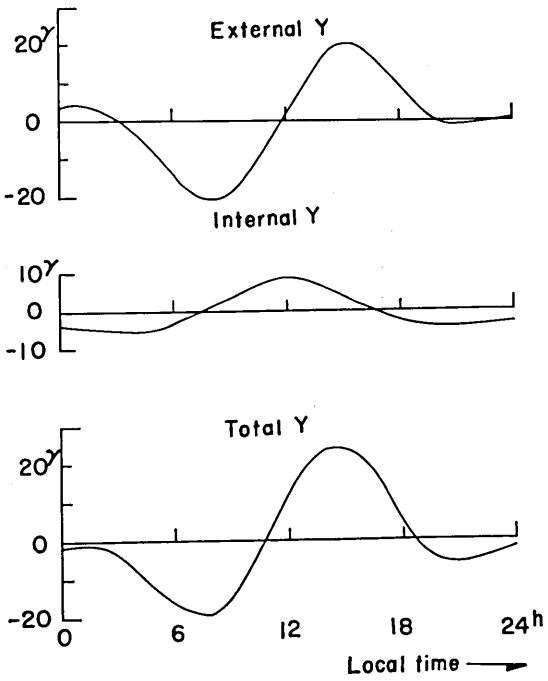


Fig. 23 b. External, internal and total $Y$ components of the $Sq$ at 160°E, 30°S.

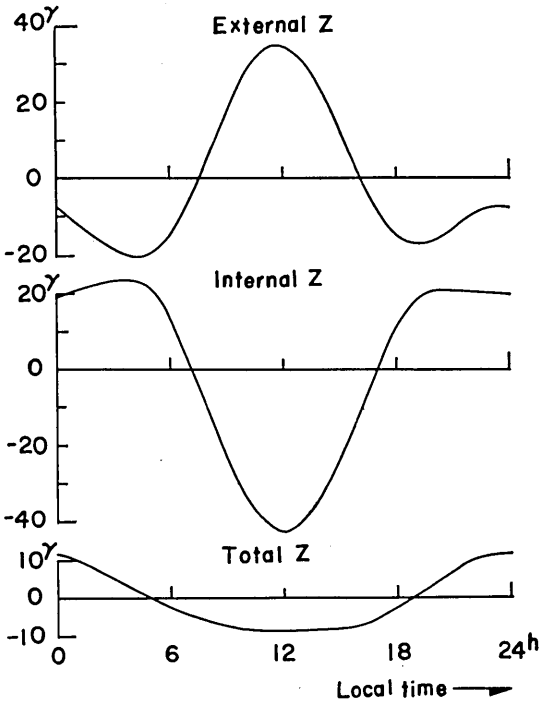


Fig. 23 c. External, internal and total $Z$ components of the $Sq$ at 180°E, 30°S.

side of South America and in the northern Pacific. These vortices change their intensities as the inducing $Sq$-field goes around the earth although their positions do not shift very much. In Fig. 22 is shown how the intensity of current function at 160°E and 30°S, which roughly corresponds to the vortex centre in the southern Pacific, changes with time. It is clearly seen in the figure that the induced current is very much stronger during the daytime than that during the nighttime.

Figs. 23 a, 23 b, and 23 c show the external, internal and total $Sq$ for the $X$, $Y$ and $Z$ components as plotted against the local time at 180°E and 30°S. It is recognized that the induced $Z$ is so strong that the inducing $Z$ is nearly cancelled out.

Attention should be drawn, however, to the fact that the present model completely ignores the conducting mantle. As pointed out by Rikitake[7], such a neglect leads to a considerable over-estimate of the ocean effect in some cases. The writer wishes to study the induction by an $Sq$ in a more realistic model in which account of the conducting mantle will be properly taken in a later paper.

Table 9 a. Changes in $K_n^{mC}(t)$'s.

| $t$ | $K_1^{0C}$ | $K_1^{1C}$ | $K_2^{0C}$ | $K_2^{1C}$ | $K_2^{2C}$ | $K_3^{0C}$ | $K_3^{1C}$ | $K_3^{2C}$ | $K_3^{3C}$ |
|---|---|---|---|---|---|---|---|---|---|
| sec. | | | | | | | | | |
| 0 | 0.11697 | 0.00849 | 0 | 0 | 0 | 0 | 0 | 0 | 0 |
| 50 | 0.06270 | 0.00853 | −0.01388 | −0.00693 | −0.00198 | −0.00170 | −0.00207 | 0.00023 | −0.00012 |
| 100 | 0.03825 | 0.00625 | −0.01185 | −0.00954 | −0.00273 | 0.00040 | −0.00318 | 0.00066 | −0.00017 |
| 200 | 0.02442 | 0.00228 | −0.00562 | −0.01038 | −0.00350 | 0.00003 | −0.00364 | 0.00116 | −0.00013 |
| 300 | 0.02263 | 0.00114 | −0.00349 | −0.01005 | −0.00392 | −0.00042 | −0.00350 | 0.00135 | −0.00007 |
| 400 | 0.02231 | 0.00128 | −0.00298 | −0.00973 | −0.00418 | −0.00039 | −0.00339 | 0.00142 | −0.00005 |
| 500 | 0.02204 | 0.00174 | −0.00281 | −0.00951 | −0.00435 | −0.00026 | −0.00335 | 0.00145 | −0.00003 |
| 600 | 0.02175 | 0.00221 | −0.00271 | −0.00935 | −0.00448 | −0.00015 | −0.00333 | 0.00147 | −0.00003 |

Table 9 b. Changes in $K_n^{mS}(t)$'s.

| $t$ | $K_1^{1S}$ | $K_2^{1S}$ | $K_2^{2S}$ | $K_3^{1S}$ | $K_3^{2S}$ | $K_3^{3S}$ |
|---|---|---|---|---|---|---|
| 0 sec. | −0.02223 | 0 | 0 | 0 | 0 | 0 |
| 50 | −0.01355 | 0.00159 | 0.00251 | −0.00120 | 0.00018 | −0.00008 |
| 100 | −0.00970 | 0.00132 | 0.00351 | −0.00091 | 0.00001 | −0.00004 |
| 200 | −0.00544 | 0.00105 | 0.00361 | −0.00019 | −0.00038 | 0.00003 |
| 300 | −0.00389 | 0.00108 | 0.00333 | 0.00003 | −0.00054 | 0.00005 |
| 400 | −0.00342 | 0.00112 | 0.00316 | 0.00009 | −0.00059 | 0.00006 |
| 500 | −0.00330 | 0.00114 | 0.00305 | 0.00011 | −0.00062 | 0.00008 |
| 600 | −0.00328 | 0.00116 | 0.00298 | 0.00012 | −0.00063 | 0.00009 |

*2-7. Free decay of the induced currents*

As an example of aperiodic induction in the land-sea model, the free decay of electric currents induced in the model by a sudden change in a uniform magnetic field parallel to the geomagnetic axis will be studied in this section. Assuming a step-function type jump of unit amplitude of the external field, it is obvious that a current system is excited at $t=0$ in such a way that the vertical field at the surface is completely cancelled. The only non-zero current function coefficient at that instant is given as

$$K_1^{0C}=0.116970, \quad K_1^{1C}=0.008490, \quad K_1^{1S}=-0.022232.$$

For $t>0$, successive computations of the coefficients according to (54) and (56) are carried out by taking $\Delta t$ as 1 sec. In Tables 9 a and 9 b are indicated the coefficients at various epochs.

The changes in the main current function coefficients are graphically

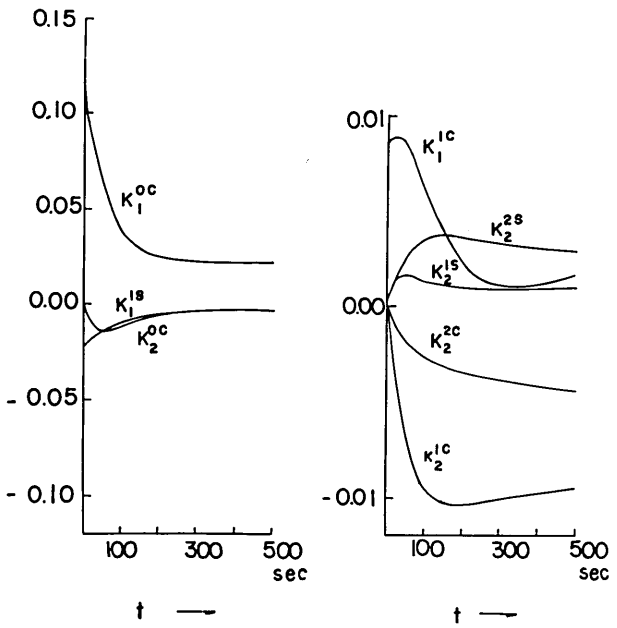


Fig. 24. Changes in the main current function coefficients in units of the inducing field amplitude.

shown in Fig. 24, too. We see that the decay of $K_1^{0C}$ is extremely slow after $t=300$ sec. or so. During the period of the fairly large decay of $K_1^{0C}$, it appears that some of the coefficients grow to a considerable extent although the decay-rate of these coefficients after their maxima are also small. Ashour[11], who studied an induction in a circular disk, reached a conclusion that the decay-time of the induced current in a vast ocean is very large. He estimated that the time-constant for a circular ocean having a 5000 km radius and a 5000 m depth amounts to 6.5 hours. Although it is difficult to perform the successive calculations for a large value of $t$ because of the accumulation of computational errors, the present results harmonize with Ashour's conclusion that a vast ocean has a very large time-constant.

In Figs. 25 a, 25 b, 25 c, 25 d and 25 e are illustrated the induced current patterns for $t=0$, 50, 100, 300, and 600 sec. respectively. The currents tend to be deflected from the low-conducting continents as time goes on, while the currents flowing in the high-conducting oceanic parts do not dissipate very much. It is therefore observed that current-flows

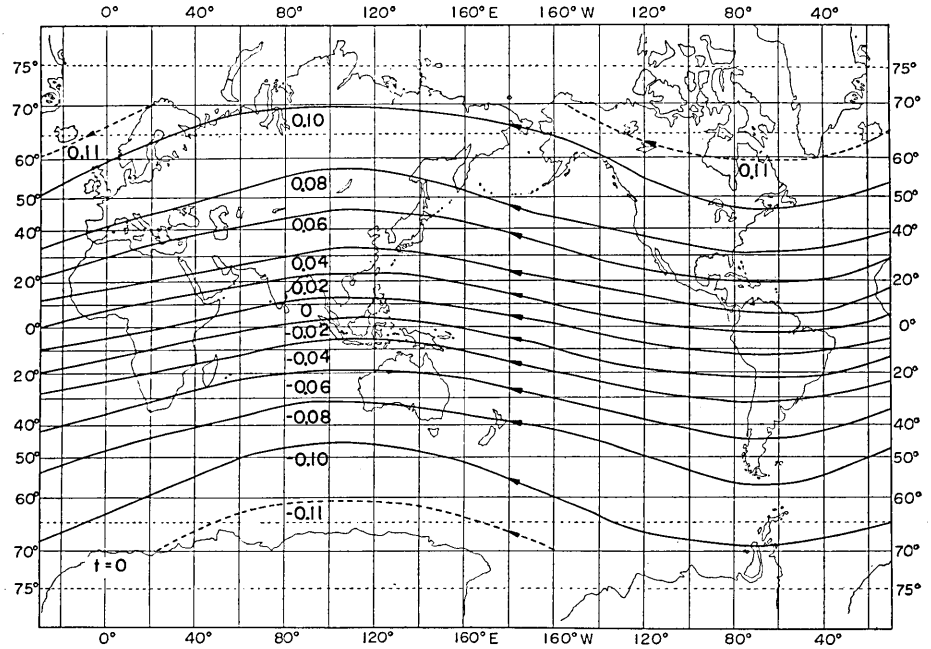


Fig. 25 a. Induced current lines in units of the inducing field amplitude at $t=0$.

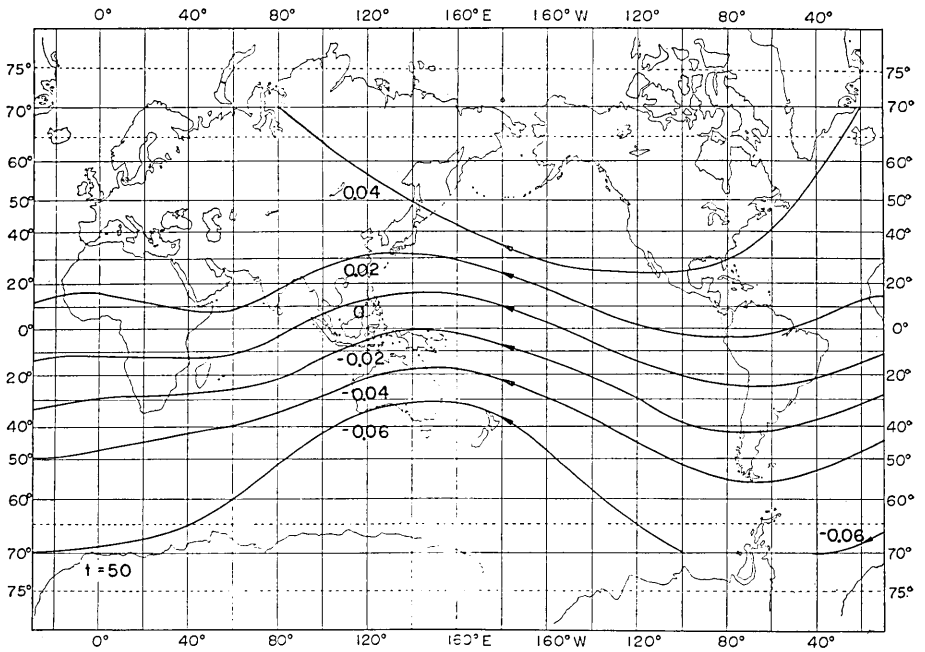


Fig. 25 b. Induced current lines at $t=50$ sec.

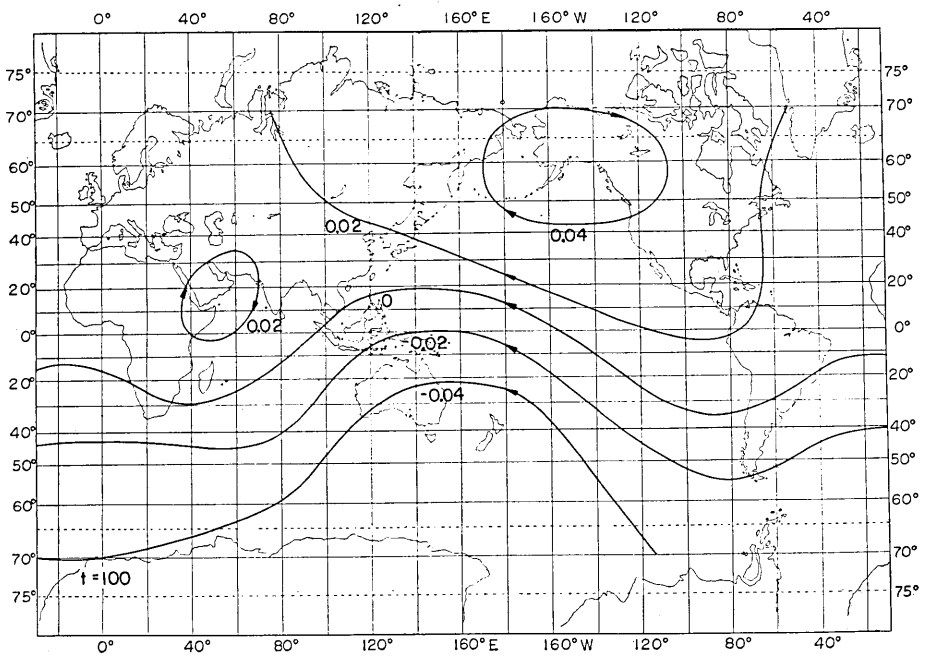


Fig. 25 c. Induced current lines at $t=100$ sec.

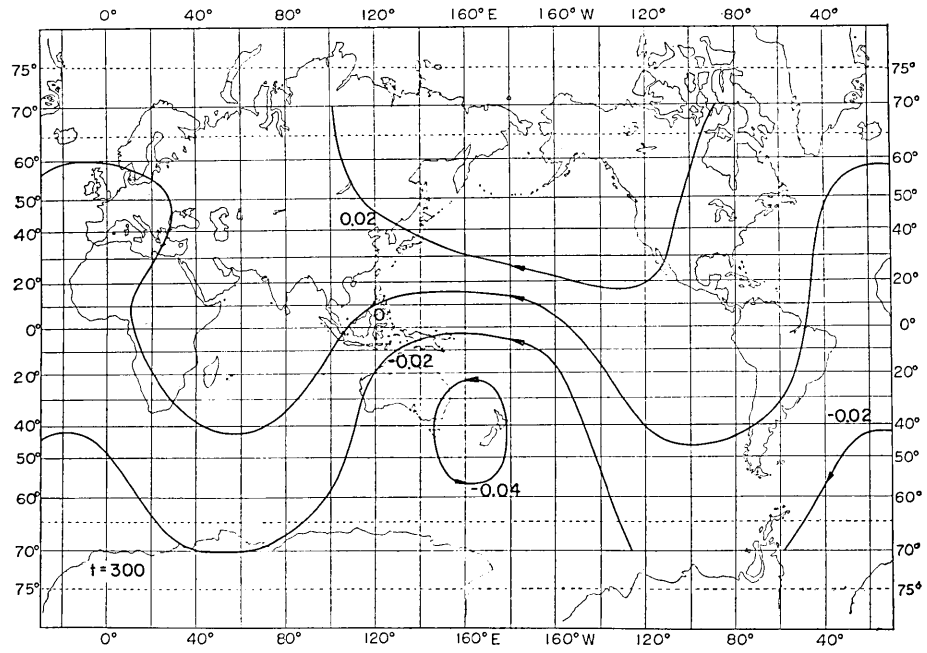


Fig. 25 d. Induced current lines at $t=300$ sec.

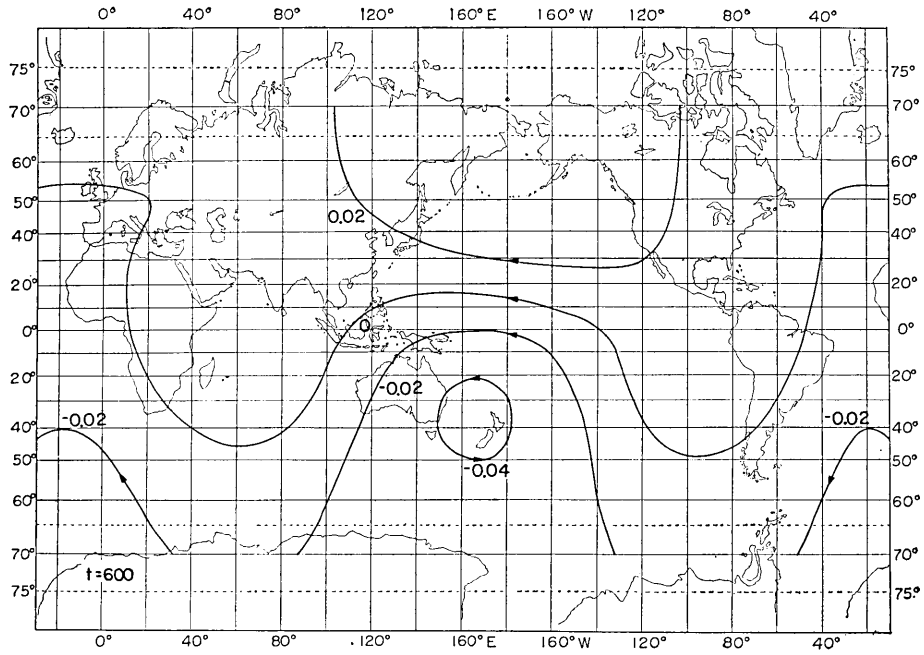


Fig. 25 e. Induced current lines at $t=600$ sec.

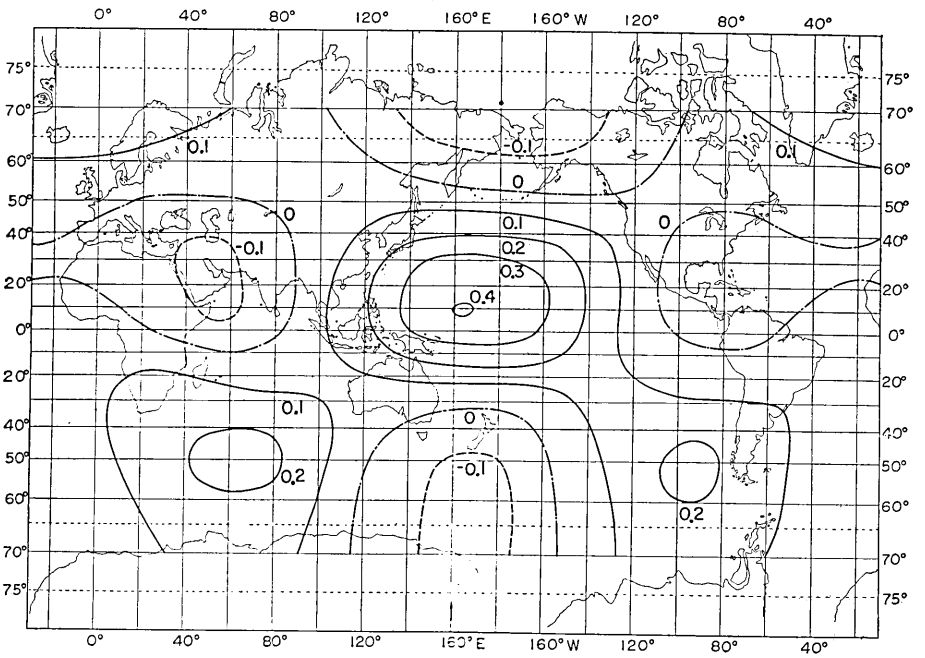


Fig. 26 a. The induced $X$ fields in units of the inducing field amplitude at $t=300$ sec.

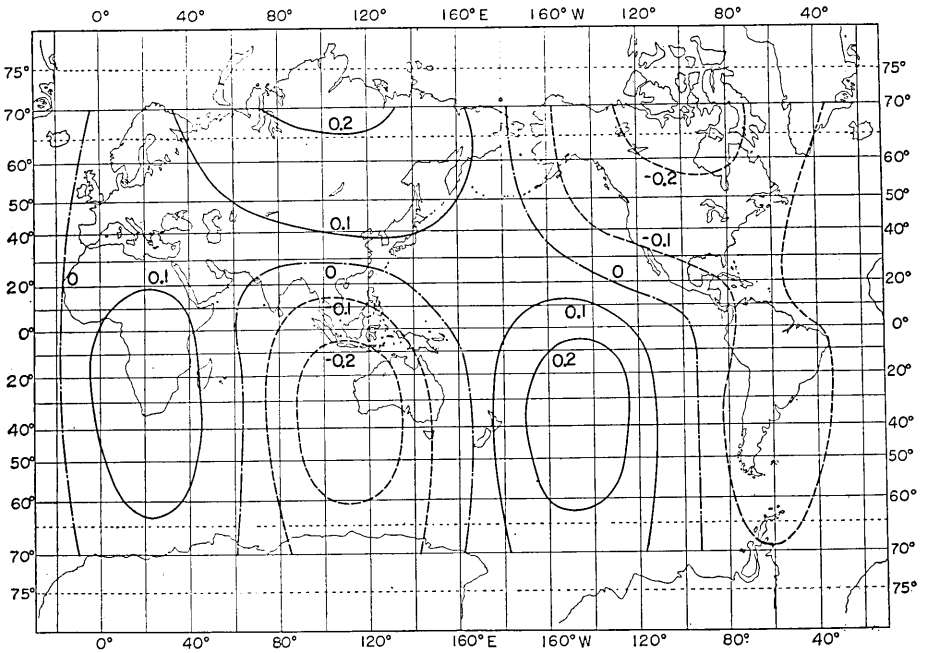


Fig. 26 b. The induced $Y$ fields at $t=300$ sec.

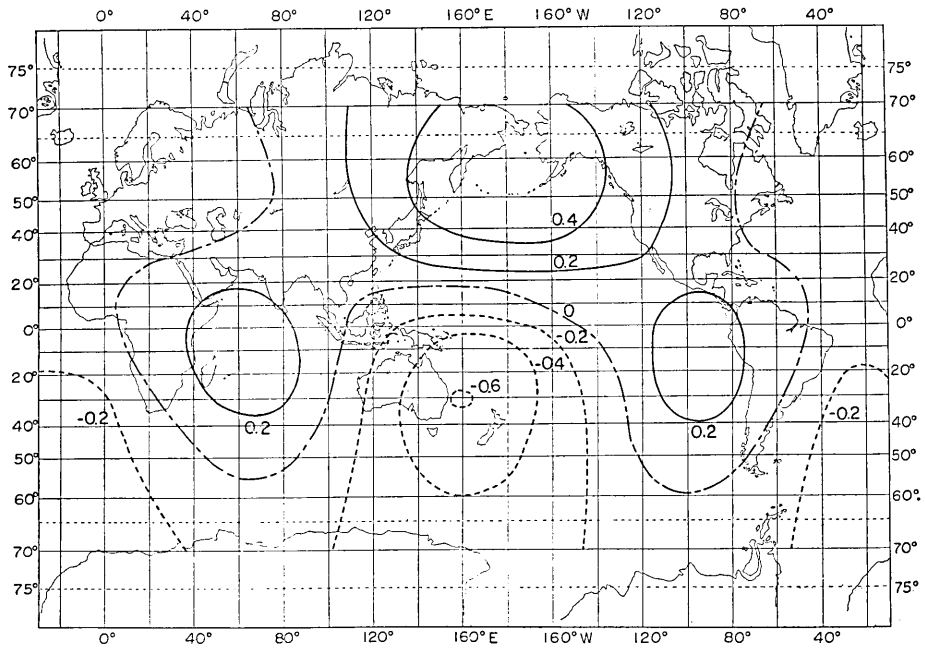


Fig. 26 c. The induced $Z$ fields at $t=300$ sec.

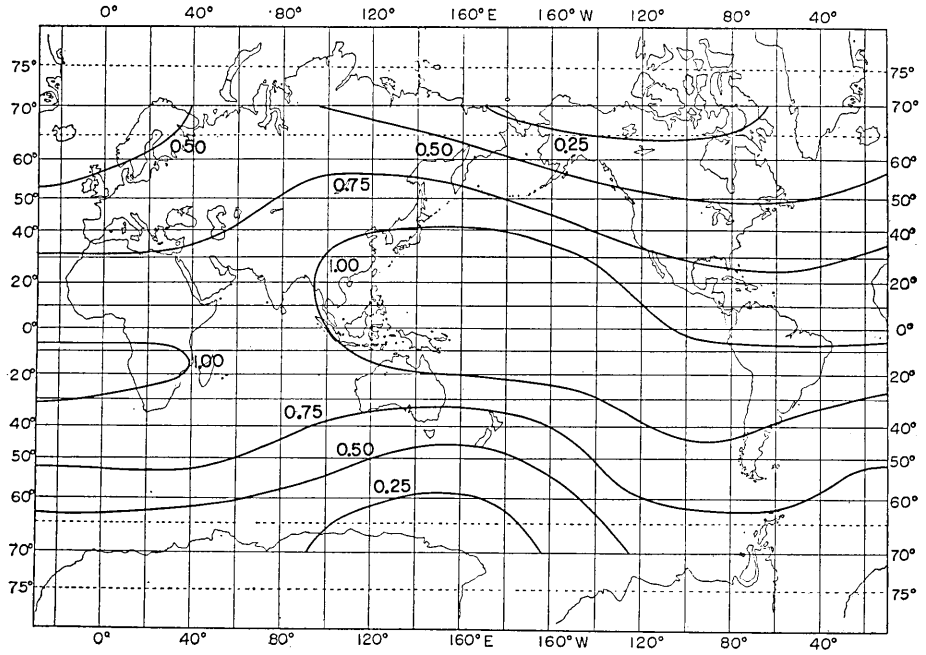


Fig. 27 a. The total $X$ fields at $t=300$ sec.

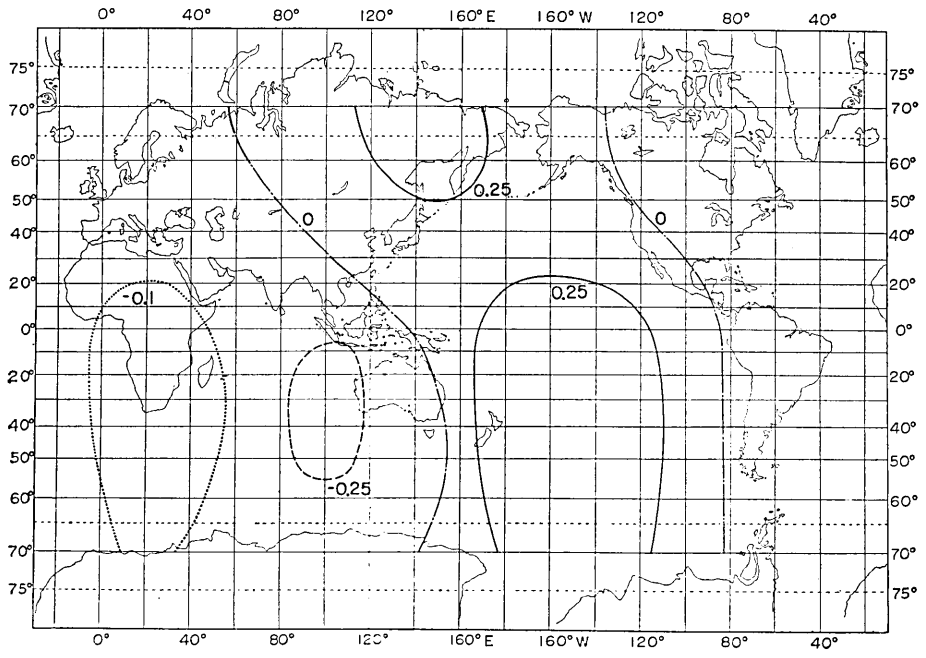


Fig. 27 b. The total $Y$ fields at $t=300$ sec.

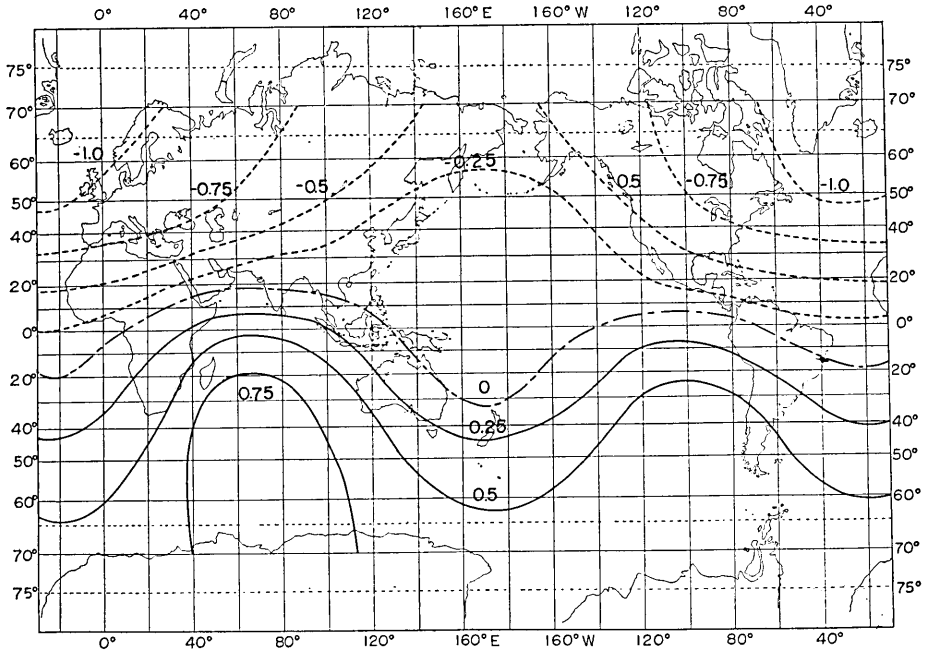


Fig. 27 c. The total $Z$ fields at $t=300$ sec.

along the peripheries of the continents and current-encirclings in the oceans prevail after some time, say for $t$ larger than 300 sec. The mean current intensity is of course subjected to a weakening.

The magnetic field components produced by these induced currents can readily be calculated. As it is tedious to illustrate all of them, only the $X$ (northward), $Y$ (eastward) and $Z$ (downward) component at $t=$ 300 sec. are shown in Figs. 26 a, 26 b and 26 c. Attention should be drawn to the fact that $Z$-component at some of the centres of current vortices reaches some 60 per cent of the inducing field.

The magnetic field components actually observed on the earth's surface are readily calculated by adding the external field to the induced field. Figs. 27 a, 27 b and 27 c show the field distribution over the earth. We see in the figures that $\Delta Z$ is negative or upward in Europe and North America and that $\Delta Z$ is positive or downward in the North and Southeast Pacific and Indian Oceans.

Maeda et al[27] examined *s.s.c*'s during the 1957-1958 IGY (Interna-

27) R. MAEDA, T. RIKITAKE and T. NAGATA, *J. Geomag. Geoelectr.*, **17** (1965), 69-93.

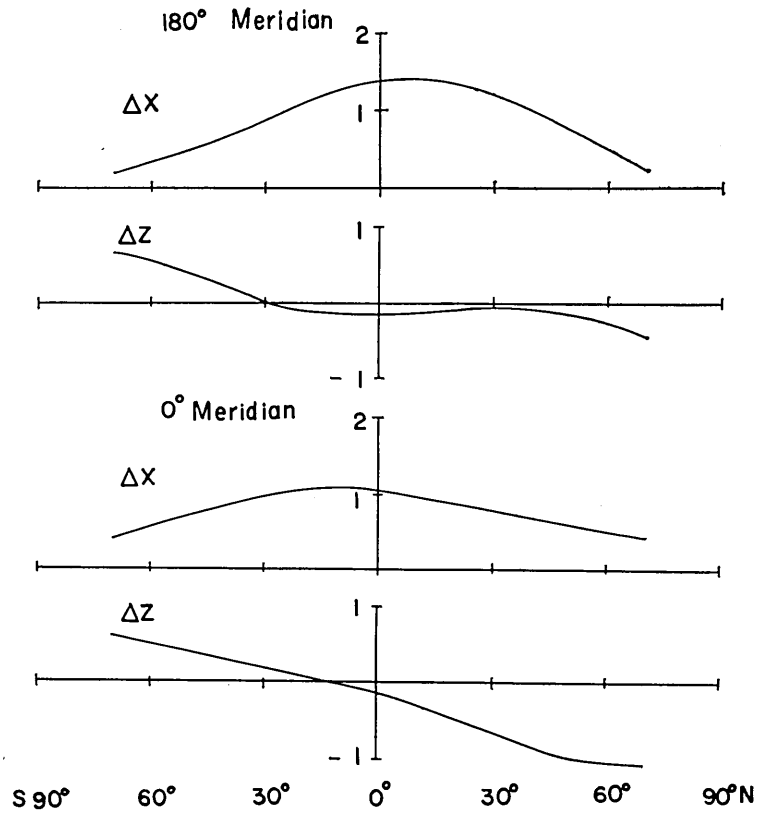


Fig. 28. The total $X$ and $Z$ fields along the 0° and 180° meridians.

tional Geophysical Year), and found that $\Delta Z/\Delta X$ and $\Delta Y/\Delta X$ for an observatory usually take on constant signs. Such a tendency is thought to be strongly affected by the high-conducting oceans as well as the underground conductivity anomalies. The distribution of the sings of $\Delta Z$ and $\Delta Y$ do not completely concide with that shown in Figs. 27 b and 27 c. But the agreements as observed in Europe and South America should be noted. $\Delta X$ and $\Delta Z$ along the 0° and 180° meridians are shown in Fig. 28 in which we observe considerable differences in the distribution of $\Delta X$ and $\Delta Z$ between the two meridians. It is therefore seen that the distribution of a rapid change like *s.s.c.* could be very complicated. Since the present model does not involve the high-conducting mantle below a depth of a few hundred kilometers, it would be of no use to compare the actually observed signs to the calculated ones. As has been emphasized by Rikitake[7,8],[9], the coupling between the surface

conductor and the conducting mantle is important in this kind of induction problem. A detailed comparison between the observed results and the calculated ones should be performed after we take the influence of the conducting mantle properly into account.

### 3. Discussion about the induction in the non-uniform spherical sheet

A tendency for the induced currents to deflect from the low-conducting continental areas is well demonstrated in the induction in the present model. Consequently, the currents tend to encircle over the oceanic areas. It is interesting to note that the centres of current vortex appear at almost the same positions for any inducing fields, so that large induced $\Delta Z$ should be observed over the North and South Pacific, Indian Oceans and off the Pacific coast of Peru. As very few magnetic observatories exist in these parts of the world, no comparison between the calculated and observed results are made.

It has been demonstrated by Rikitake[7] that the currents induced in a hemispherical ocean become a few times smaller than those estimated for the model in which no account is taken of the electromagnetic coupling between the ocean and the conducting mantle. It would be of little use, therefore, to undertake a detailed comparison between the observed and calculated results until the effect of the conducting mantle is properly taken into account.

## General discussion and conclusions

It has been shown in this paper that electromagnetic inductions in non-uniform plane and spherical sheets that simulate a realistic land-ocean conductivity contrast can be approximately tackled by making use of a high-speed computer. The present method essentially bases on obtaining the coefficients of spherical harmonic function of finite number, so that it is obvious that the degree of approximation for the induced currents and fields is considerably low if the model involves very sharp conductivity contrasts. But it is believed that the gradual transitions from land to sea as treated in Part 1 and the over-all surface conductivity distribution as given in Part 2 may provide models which do not give rise to unreasonably large amplitude of higher harmonic functions.

All through the present study, deflection of the induced currents from the low-conducting portions of the models is well demonstrated.

In Part 1 it is suggested that an anomalous magnetic field like a reversal in $\Delta Z$ takes place only over the deep ocean provided a gradual increase in the sea-depth is taken into account. One of the important conclusions in Part 2 would certainly be the fact that the centres of the induced current vortex appear at almost the same positions.

The existence of a high-conducting mantle below a depth of a few hundred kilometers has been well accepted. It is certain that the electromagnetic coupling between the surface conductor and the conducting mantle largely modifies the induced currents in the surface sheet. The effect of such a coupling will be studied in a later paper.

In conclusion the writer thanks Dr. Y. Hagiwara for his help in compiling the computer programmes. Most of the calculations involved in this paper were done on a HITAC 5020 computer at the Computer Centre, University of Tokyo and also on an IBM 7090 computer at the IBM Data Processing Centre through the Project UNICON.

---

## 54. 不均質薄層の電磁感応

地震研究所　力武常次

任意の不均質電気伝導度分布をもつ平面および球面薄層中の電磁感応を調べるためのプログラムをつくった．海岸から大洋底に至る深さの漸増を考慮した平面モデルでは，深海部分に感応電流が集中し，磁場の反転等の異常も起こることがある．

地球表面全体にわたる電気伝導度分布を近似する球面モデルについては，感応電流が大陸をさけ，大洋を流れるようになる．南太平洋では特に電流の encircling が顕著である．*Sq*, *s. s. c.* などがこの感応電流のつくる磁場にかなり影響されるが，マントルの導電的部分との電磁結合はこの影響を弱めるであろう．

---